



University of Dundee

Newmark sliding block model for pile-reinforced slopes under earthquake loading

Al-Defae, A. H.; Knappett, Jonathan

Published in:
Soil Dynamics and Earthquake Engineering

DOI:
[10.1016/j.soildyn.2015.04.013](https://doi.org/10.1016/j.soildyn.2015.04.013)

Publication date:
2015

Document Version
Peer reviewed version

[Link to publication in Discovery Research Portal](#)

Citation for published version (APA):
Al-Defae, A. H., & Knappett, J. A. (2015). Newmark sliding block model for pile-reinforced slopes under earthquake loading. *Soil Dynamics and Earthquake Engineering*, 75, 265-278. DOI: 10.1016/j.soildyn.2015.04.013

General rights

Copyright and moral rights for the publications made accessible in Discovery Research Portal are retained by the authors and/or other copyright owners and it is a condition of accessing publications that users recognise and abide by the legal requirements associated with these rights.

- Users may download and print one copy of any publication from Discovery Research Portal for the purpose of private study or research.
- You may not further distribute the material or use it for any profit-making activity or commercial gain.
- You may freely distribute the URL identifying the publication in the public portal.

Take down policy

If you believe that this document breaches copyright please contact us providing details, and we will remove access to the work immediately and investigate your claim.

Elsevier Editorial System(tm) for Soil Dynamics and Earthquake Engineering
Manuscript Draft

Manuscript Number: SOILDYN-D-14-00245R2

Title: Newmark sliding block model for pile-reinforced slopes under earthquake loading

Article Type: Research Paper

Keywords: Slope stability; Earthquakes; Centrifuge models; Piles; Sands; Embankments.

Corresponding Author: Dr. Jonathan Knappett, MA MEng PhD

Corresponding Author's Institution: University of Dundee

First Author: Asad H Al-Defae, BSc PhD

Order of Authors: Asad H Al-Defae, BSc PhD; Jonathan Knappett, MA MEng PhD

© 2015. This manuscript version is made available under the CC-BY-NC-ND 4.0 license <http://creativecommons.org/licenses/by-nc-nd/4.0/>



School of Engineering, Physics and Mathematics

14th April, 2015

To the Editor in Chief,

Re: Submission of revised manuscript for publication in Soil Dynamics and Earthquake Engineering:

“Newmark sliding block model for pile-reinforced slopes under earthquake loading” (Revision 2)

Dean
Professor T J Newman

School Secretary
Rebecca Leiper

Assistant School Secretary
Rachel Smith

Director of Undergraduate Studies
Mr Andrew Munns

Finance Officer
Mrs Karen Wilson

Secretarial Staff
Miss Louise Allardice
Miss Jennifer Colliar
Mrs Shirley Fox
Miss Linda Rannie
Mrs Prue Reid
Mrs Ann Robertson

My co-author and I hereby submit the above named revised manuscript for publication in Soil Dynamics and Earthquake Engineering as a full technical paper. We have included a full response to the reviewers' additional minor comments.

We hereby confirm that the paper is entirely original and is not under consideration by any other journal.

Should you require any further information, please do not hesitate to contact me on j.a.knappett@dundee.ac.uk.

Yours sincerely,

A handwritten signature in black ink, appearing to read 'J. Knappett'.

Jonathan Knappett (Corresponding author)
Senior Lecturer

Detailed Response to Reviewers

Reviewer #1: Responses to my review comments on the original paper are accepted. The following comments refer to the Rev 1 of the paper:

1. Line 37: Suggest replacing the word "conglomerate" with "combined" because I suspect that a conglomerate soil-pile interaction model will be interpreted by some as assessing soil-pile interaction in a conglomerate soil. I realize that I used this term in my initial review comments but in the paper itself I think it is too risky given the usual use of this term in the geological context in our profession.

We have replaced "conglomerate" with "combined" as suggested.

2. Line 74: Suggest replacing the word "complimentary" with "more".

We thank the reviewer for spotting this misspelling. We had meant "complementary" as we believe the simplified model would be useful when combined as a two stage analysis with Newmark first, followed by FEM, as outlined in lines 79-81. We have therefore changed the word to "complementary".

3. Line 193: Two relationships are presented for Equation (7) but only one applies (the second one) - need to delete the first relationship given for p.

We think this was due to a hidden equation object (it does not appear in our word file, but becomes visible when converted to pdf). We believe this has now been corrected.

4. Line 194: Delete the letter "p" preceding "Pi".

Corrected as suggested.

5. Line 200: Two relationships are presented for Equation (8) but only one applies (the second one) - need to delete the first relationship given for pult.

We think this was due to a hidden equation object (it does not appear in our word file, but becomes visible when converted to pdf). We believe this has now been corrected.

6. Line 201: Delete the letter "d" preceding "Deq".

Corrected as suggested.

7. Line 512: Suggest replacing the word "conglomerate" with "combined" as per my reasoning given in Comment #1.

We have replaced "conglomerate" with "combined" as suggested.

Highlights:

- A sliding block method incorporating strain-dependent pile resistance is presented.
- Discontinuity Layout Optimisation (DLO) was used to find slip plane location.
- The sliding block method was validated against centrifuge test data.
- Slope deformations and maximum pile moments were well predicted.
- The method was also validated for multiple sequential motions (aftershocks).

30 **Abstract**

31 Recent studies have demonstrated that the use of a discretely-spaced row of piles can be
32 effective in reducing the deformations of slopes in earthquakes. In this paper, an
33 approximate strain-dependant Newmark sliding-block procedure for pile-reinforced slopes
34 has been developed, for use in analysis and design of the piling scheme, and the model is
35 validated against centrifuge test data. The interaction of the pile within the slipping soil was
36 idealised using a non-linear elasto-plastic (P - y) model, while the interaction within the
37 underlying stable soil was modelled using an elastic response model in which (degraded)
38 soil stiffness is selected for an appropriate amount of shear strain. This **combined** soil-pile
39 interaction model was incorporated into the improved Newmark methodology for
40 unreinforced slopes presented by Al-defae et al. [1], so that the final method additionally
41 incorporates strain-dependent geometric hardening (slope re-grading). When combined with
42 the strain-dependent pile resistance, the method is therefore applicable to analysis of both
43 the mainshock and subsequent aftershocks acting on the deformed slope. It was observed
44 that the single pile resistance is mobilised rapidly at the start of a strong earthquake and that
45 this and the permanent slope deformation are therefore strongly influenced by pile stiffness
46 properties, pile spacing and the depth of the slip surface. The model shows good agreement
47 with the centrifuge test data in terms of the prediction of permanent deformation at the crest
48 of the slope (important in design for selecting an appropriate pile layout/spacing i.e. S/B) and
49 in terms of the maximum permanent bending moments induced in the piles (important for
50 appropriate structural detailing of the piles), so long as the slip surface depth can be
51 accurately predicted. A method for doing this, based on limit analysis, is also presented and
52 validated.

53

54 **Keywords:** Slopes, Piles, Sand, Analytical modelling, Centrifuge modelling,

55

56 1. Introduction

57 The technique of slope stabilisation by piling is widely used by geotechnical engineers
58 to utilise the bending response of the pile to stabilise the sliding mass by coupling this to
59 stronger stable strata below. The piling would typically be installed as a discretely-spaced
60 pile row running along the length of the slope at a centre-to-centre spacing, S , with a
61 sufficient length to allow them to pass through the unstable slipping soil mass and become
62 anchored in the underlying stable soil. In the pre-failure stage the piles promote arching of
63 stresses between adjacent piles which improves stability [2, 3]. If the soil mass slips (the
64 piles being designed to remain elastic), the ground movements generate relative soil-pile
65 displacement, which in turn leads to the mobilisation of lateral earth pressures along the
66 piles, and additional resistance due to the subsequent pile bending.

67 In the analysis and design of such piling schemes, it is important to be able to
68 determine (i) the reductions in seismic displacement for a given pile arrangement (e.g.
69 normalised spacing S/B , where B is the pile width or diameter) so that the piling can be
70 designed to give the required improvement to the geotechnical performance (i.e. reduction in
71 slip); and (ii) internal forces (e.g. bending moments) within the piles, so that they can be
72 structurally detailed. Analytical solutions have been developed for the analysis of pile-slope
73 systems under static loads (e.g. [4 – 6]). Kourkoulis et al. [7] have demonstrated the use of
74 Finite Element (FE) modelling for analysing the performance of piled slopes under seismic
75 loading, but it would be useful in preliminary design phases to have a **complementary** simple
76 model which can provide the required response parameters rapidly without requiring the use
77 of finite element software. Such a tool would be useful for (i) conducting large parametric
78 studies; (ii) use in performance-based earthquake engineering where statistical approaches
79 and Monte-Carlo simulation may be necessary; and (iii) in refining the design before more
80 detailed FE modelling is conducted to verify final performance, thereby potentially reducing
81 the amount of FE modelling which is required.

82 In this paper, a simplified approximate soil-pile interaction (SPI) model for determining
83 mobilised pile resistance with soil slip is formulated for piles passing through a slipping soil
84 mass and anchored into stable soil beneath. This is then incorporated within a Newmark
85 sliding block analysis [8, 9] through an enhanced yield acceleration considering the forces
86 (including mobilised pile resistance) acting on the slipping soil mass. In this case, an
87 improved Newmark analysis methodology, developed recently by Al-defae et al. [1], is used
88 with this yield acceleration. This methodology additionally incorporates strain-dependent
89 geometric hardening (slope re-grading) through updating the instantaneous slope angle in
90 each time step. As the soil-pile resistance and slope geometry is tracked throughout the
91 analysis as a function of soil slip (i.e. strain), the new model is implicitly suitable for also
92 estimating performance in subsequent accompanying aftershocks which may occur on an
93 already-damaged slope (i.e. before it has been repaired). The model developed is validated
94 against centrifuge test data for pile-reinforced sandy slopes reported previously by Al-defae
95 and Knappett [10].

96 **2. Sliding block procedure for pile-reinforced slopes**

97 *2.1 Formulation*

98 The limit equilibrium formulation for the yield acceleration of an infinite slope
99 developed by Al-defae et al. [1], which includes strain-dependent geometric hardening of the
100 slope, is here modified to incorporate the additional component of resistance to sliding
101 provided by the piles. For slip of a moving mass of soil of length L , width S , unit weight γ
102 and with a slip plane depth of z_{slip} beneath the slope surface, the applied downslope shear
103 stress from Figure 1 is:

$$104 \quad \tau_{applied} = \gamma z_{slip} \sin \beta \cos \beta + k_h \gamma z_{slip} \cos^2 \beta \quad (1)$$

105 where the first term relates to the static shear stress due to the ground slope, and the
 106 second term relates to the additional peak dynamic downslope shear stress induced by the
 107 earthquake shaking. The total shear resistance to this applied shear stress is given by:

$$\begin{aligned}
 \tau_{ult} &= c' + \sigma' \tan \phi' + \frac{P}{LS} \cos \beta \\
 &= c' + (\gamma z_{slip} \cos^2 \beta - k_h \gamma z_{slip} \sin \beta \cos \beta - u) \tan \phi' + \frac{P}{LS} \cos \beta
 \end{aligned}
 \tag{2}$$

109 where P is the horizontal shear resistance force provided by a single pile, determined from
 110 the soil-pile interaction model presented in Section 3. The soil yields when $\tau_{applied} = \tau_{ult}$.
 111 The value of k_h at which this occurs (i.e. the yield acceleration, k_{hy}) can be determined from
 112 Equations (1) and (2) as:

$$k_{hy} = \frac{c' + (\gamma z_{slip} \cos^2 \beta - u) \tan \phi' - \gamma z_{slip} \sin \beta \cos \beta + \frac{P}{LS} \cos \beta}{\gamma z_{slip} \cos^2 \beta + \gamma z_{slip} \sin \beta \cos \beta \tan \phi'}
 \tag{3}$$

114 In Equation (3), u' , β , L and P are functions of shear strain (ϵ_s) on the shear plane due to
 115 slope displacement. Al-defae et al. [1] showed that the strain softening model of Matasovic
 116 et al. [9] can be used to describe $u'(\epsilon_s)$. A simple relationship was then developed to
 117 describe the geometric effect of an increment of slip in reducing the slope angle (β), which is
 118 shown in Figure 2. Numerically within the Newmark sliding block method, the slope angle is
 119 updated for step $i+1$ based on the slope angle (β_i) and the amount of slope-parallel slip (d_i),
 120 both from the previous step, using:

$$\beta_{i+1} = \tan^{-1} \left(\frac{H_i - d_i \sin \beta_i}{H_i \cot \beta_i + d_i \cos \beta_i} \right)
 \tag{4}$$

122 For the initial time step ($i = 0$): $d_0 = 0$, $H_i = H$ and $\beta_i = \beta_0$, as in [1]. When considering the
 123 relative contribution of a pile and the soil shear strength to the total resistance, the

124 instantaneous slip-plane length (L_i) is also required, which is related to the instantaneous
125 slope angle by:

$$126 \quad L_i = \frac{H_i}{\sin \beta_i} \quad (5)$$

127 The pile resistance (P) as a function of strain (soil slip) depends on a number of
128 parameters describing the relative soil-pile stiffness and relative soil-pile strength. Clearly, in
129 the initial stages of the analysis before any slip has taken place, the net additional resistance
130 from the piles is zero. As the soil slips, the relative displacement between the soil and the
131 pile increases, providing a progressively larger resistance to slip. Eventually, the resistance
132 from the pile will reach a maximum limiting value when either the soil yields around the pile,
133 or the pile yields structurally, whichever occurs first. In designing an arrangement of slope
134 stabilising piles, it will be desirable for the piles to remain elastic such that the soil fails
135 before the piles and the piled slope therefore has its maximum possible resistance to sliding.
136 This approach has the added benefit that once fully mobilised, the maximum soil-pile
137 resistance will remain at this maximum level for subsequent earthquakes, without the piles
138 becoming extensively damaged.

139 As the soil starts to slip, P will increase, while β will reduce, due to the effects
140 described above. Both changes will result in progressive hardening of the slope response
141 via an increase in the yield acceleration (Equation (3)). Even once the piles are providing
142 their maximum resistance, the slope response will continue to be reduced compared to the
143 unreinforced case due to (i) the constant value of P in Equation (3), so long as the soil or
144 pile are yielding in a ductile way, and (ii) the continued geometric hardening. By fully
145 incorporating the effects of strain within the model, the behaviour of a seismically damaged
146 slope during subsequent earthquakes/aftershocks can be determined by starting such an
147 analysis from the initial conditions (pile resistance, amount of slip, re-graded slope angle)
148 obtained at the end of the previous ground motion, as presented for unreinforced slopes in
149 [1].

150 *2.2 Assumptions and simplifications*

151 For small to moderate earthquakes whose peak ground acceleration magnitude is
152 close to (but larger than) k_{hy} and which will therefore have only a limited amount of slip,
153 strain-softening behaviour [9] can have a dramatic effect on computed slope displacements,
154 with k_{hy} potentially changing continuously throughout the earthquake as u' softens. In larger
155 earthquakes, where a single cycle causes sufficient slip/strain to reach critical state
156 conditions, then the strain softening model is likely to predict only a marginally smaller slip
157 compared to a standard (strain-hardening) analysis using a constant $u' = u'_{cs}$ [1]. Therefore,
158 a constant friction angle is used throughout the model in this paper. Michalowski and Shi
159 [11] showed that the deformation in sandy layers can be represented using a non-
160 associative flow rule and that an associative flow rule (normality principle) does not
161 accurately describe deformation in granular soil. Thus, in this paper, a generalised non-
162 associative condition is assumed, which is incorporated using a modified friction angle u^*
163 following [12]:

164
$$\tan \phi^* = \frac{\cos \psi' \cos \phi'_{pk}}{1 - \sin \psi' \sin \phi'_{pk}} \tan \phi'_{pk} \quad (6)$$

165 where u'_{pk} is the peak friction angle and ψ' is the angle of dilation.

166 It is also assumed, as in [1], that once the slope has deformed to a new, smaller value
167 of β the failure mechanism will continue to be of the infinite type, with a new slip surface
168 forming parallel to the new slope surface. This allows the model to be used even for the
169 case of large total slope movements (such as may accrue during a series of strong
170 aftershocks) as the displacement increment in each individual time step remains small, and
171 therefore the instantaneous failure mechanism can be represented by Figure 2 for small
172 displacements.

173 3. Soil-pile interaction (SPI) model

174 In this section, the relationship between the instantaneous amount of soil slip, y_{si} (=
175 Σd_i), and the corresponding pile resistance, P_i , is developed. This relationship, hereafter
176 termed the SPI model, will also enable the peak bending moments to subsequently be
177 derived within the piles, so that they can be appropriately detailed. Given that, as described
178 previously, the aim in design will be to ensure the piles remain undamaged, it can be
179 assumed that the soil in the slipping mass will yield around the piles. The interaction in this
180 zone of soil is here described using a single non-linear elasto-plastic P - y curve ('spring')
181 which describes the force applied on the pile by the slipping soil (and vice-versa), P_i , as a
182 function of the relative displacement between the soil and the pile ($y_{si} - y_{pi}$) at the point of
183 resultant load application. The part of the pile within the stable soil is modelled using a
184 linearised elastic response model describing the response of the pile at the point of load
185 application (y_{pi}) under the applied load P_i . This simplified conglomerate approach is shown
186 schematically in Figure 3.

187 3.1 Soil-pile interaction in slipping soil

188 P - y curves are popular for describing the non-linear relationship between soil
189 resistance and relative soil-pile deformation. O'Neill and Murchison [13] developed a
190 procedure which was subsequently adopted by the American Petroleum Institute (API) to
191 determine the load-deflection relationship (P - y curve) in sands. This method is used herein
192 within the slipping soil. The P - y curve in this procedure consists of an hyperbolic tangent
193 function to represent the non-linearity in the response. This relationship is written as:

$$194 \quad P_i = Ap_u \tanh \left[\frac{kz_{slip}}{Ap_u} (y_{si} - y_{pi}) \right] z_{slip} \quad (7)$$

195 where P_i is the resultant soil-pile reaction over the length of the pile within the slipping soil
196 mass (i.e. over a section of length z_{slip}), p_u is the ultimate soil resistance per unit length of
197 the pile (see below) at soil yield, y_{si} is the cumulative soil slip, y_{pi} is the lateral pile

198 displacement at the location of the P - y curve, k is the initial modulus of subgrade reaction
 199 and A is a factor to account for cyclic loading ($A = 0.9$ for cyclic loading; $A = 1.0$ for
 200 monotonic loading). The ultimate capacity per unit length, p_u , is calculated as:

$$201 \quad p_u = (C_1 z_{slip} + C_2 D_{eq}) \gamma' z_{slip} \quad (8)$$

202 where D_{eq} is the equivalent pile diameter (for a square pile this is assumed to be equal to
 203 the pile width, i.e. $D_{eq} = B$) and γ' is the effective unit weight of the soil ($= \gamma - \gamma_w$). The
 204 coefficients C_1 and C_2 and the initial subgrade reaction k are determined as a function of the
 205 angle of internal friction as outlined in [14] and summarised in Figure 4.

206 3.2 Soil-pile interaction in stable soil

207 In the stable soil, the soil is initially assumed to remain elastic, with the relationship
 208 between applied load and pile displacement presented by Randolph [15]. Its implementation
 209 here is shown schematically in Figure 5. It is assumed that the lateral pressure acting on the
 210 pile within the unstable soil increases approximately linearly with depth, so that the resultant
 211 horizontal force on the pile from the slipping soil (i.e. the P - y spring force) acts at a depth of
 212 $0.67z_{slip}$ below the top of the pile. This means that the pile length within the stable soil is
 213 treated as a partially embedded pile acted upon by a resultant horizontal force ($= P_i$) and
 214 moment ($= P_i \times 0.33 z_{slip}$) acting at the level of the shear plane. The resulting relationship
 215 between P_i and y_{pi} is given by:

$$217 \quad P_i = \frac{\rho_c G_c L_c}{\cos \beta_i \left(\frac{E_p}{G_c} \right)^{\frac{1}{7}} \left[0.54 + 0.40 \frac{z_{slip}}{L_c} \right]} y_{pi} \quad (9)$$

218 where:

$$219 \quad E_p = \frac{64EI}{\pi D_{eq}^4} \quad (10)$$

$$L_c = D_{eq} \left(\frac{E_p}{G_c} \right)^{\frac{2}{7}} \quad (11)$$

$$G_c = \bar{G}_{Lc} (1 + 0.75\nu) \quad (12)$$

$$\rho_c = \frac{G(z_{slip} + L_c/4)}{\bar{G}_{Lc}} \quad (13)$$

The parameter \bar{G}_{Lc} is the median value of the operative shear modulus over the critical length (L_c), i.e. the value of G at a depth of $L_c/2$, and ρ_c is an homogeneity factor describing the variation of G with depth. The method can therefore account for (linear) variation of soil shear modulus with depth within the stable soil, and pile sections of any bending stiffness and cross-section EI (through use of an equivalent elastic circular pile of Young's Modulus E_p , Equation 10).

The key modification made to this existing model in this paper is that the 'operative' shear modulus (G) is reduced to account for the effects of cyclic shearing in the free-field (which is here assumed to also approximate the cyclic effects in the near-field soil). The analytical estimation of this G - z relationship is described in Section 3.3. To use Equations (11) – (13) some iteration is required due to the inter-relationships between L_c and G_c . In practice an initial value of L_c is assumed and used to determine G_c . This value of G_c is then used in Equation (11) to calculate an improved estimate of L_c . This changes G_c (c.f. Figure 5). The procedure is repeated until the values of G_c and L_c are consistent with each other.

3.3 Estimation of operative shear modulus in stable soil

The 'operative' shear modulus (G - z relationship) required for the 'stable' part of the SPI model can be determined based on the initial small-strain shear modulus (G_o) for the soil before cyclic loading (from Hardin and Drnevich [16] – Equation 14) and the variation of

241 RMS average cyclic shear stress (τ_{av}) and cyclic shear strain ($\epsilon_{s,cyc}$) with depth during the
 242 earthquake (Equation 15):

$$243 \quad G_o = 100 \left[\frac{(3-e)^2}{1+e} \right] (p'_0)^{0.5} \quad (14)$$

$$244 \quad \frac{G}{G_o} = \frac{\tau_{av}}{G_o \epsilon_{s,cyc}} \quad (15)$$

245 where $p'_0 = (1 + 2K_0)\sigma'_{v0}/3$ is the initial mean confining stress (K_0 being the coefficient of
 246 lateral earth pressure) and e is the void ratio. The cyclic shear stress is estimated using an
 247 equation proposed by Seed and Idriss [17] where the RMS average cyclic shear stress
 248 caused by earthquake was estimated as approximately 0.65 times the peak shear stress:

$$249 \quad \tau_{av} = 0.65 \left(\frac{a_{max}}{g} \right) \sigma_{v0} r_d \quad (16)$$

250 where a_{max} is the peak ground acceleration at the soil surface, g is the acceleration due to
 251 gravity, σ_{v0} is the total overburden stress, and r_d is a stress reduction coefficient which is
 252 here determined following [18]:

$$253 \quad r_d = e^{[\alpha_1(z) + \alpha_2(z) \cdot M_w]} \quad (17)$$

254 where M_w is the earthquake magnitude, z is the depth below ground surface in meters and:

$$255 \quad \alpha_1 = -1.012 - 1.126 \sin \left(\frac{z}{11.73} + 5.133 \right) \quad (18)$$

$$256 \quad \alpha_2 = 0.106 + 0.118 \sin \left(\frac{z}{11.28} + 5.142 \right) \quad (19)$$

257 The cyclic shear strain ($\epsilon_{s,cyc}$) is estimated using Equation (20) as proposed by Pradel [19]:

258
$$\varepsilon_{s,cyc} (\%) = \left\{ \frac{1 + a.e^{(b.\tau_{av.}/G_0)}}{1 + a} \right\} \frac{\tau_{av.}}{G_0} \times 100 \quad (20)$$

259 where

260
$$a = 0.0389 \left(\frac{p'_0}{p_a} \right) + 0.124 \quad (21)$$

261
$$b = 6400 \left(\frac{p'_0}{p_a} \right)^{-0.6} \quad (22)$$

262 In Equations (21) – (22) p_a is atmospheric pressure (100 kPa).

263 *3.4 Pile spacing effects (pile ‘shadowing’) and local non-linearity in stable soil*

264 When using piles in a closely spaced pile row, the zones of soil into which the piles
 265 displace relative to the soil may overlap, resulting in a reduction in the resistive force
 266 available due to ‘shadowing’ [3]. This is accounted for in the present analysis by applying
 267 the p -multiplier concept, i.e. by multiplying the values of P in the SPI model by a factor p_m
 268 between 0 – 1, dependent on the pile spacing. Previously proposed p -multipliers for circular
 269 piles are summarised in Figure 6. A simple bi-linear approximate relationship was inferred
 270 from this data for use within the SPI model, having a cut-off spacing of $5B$, given by:

271
$$p_m = \begin{cases} 0.235 \frac{S}{B} - 0.168 & \frac{S}{B} \leq 5.0 \\ 1.0 & \frac{S}{B} \geq 5.0 \end{cases} \quad (23)$$

272 It is here assumed that Equation (23) applies to both circular piles of diameter B and square
 273 piles of side B (as previously assumed in Equations (8), (10 and (11)).

274 While the slipping soil mass incorporates elasto-plastic behaviour through the P - y
 275 approach (Equation 7), the stable soil model presented in Section 3.2 is based on a purely
 276 elastic soil response to relative soil-pile movement (albeit in a soil medium which has

277 reduced operative stiffness due to shaking – Section 3.3). In reality, however, there may be
 278 a modest amount of non-linearity in the stable mass just below the location of the slip plane
 279 where the relative soil-pile deformations due to pile deflection will be larger [21]. To maintain
 280 the simplicity of the method, this effect is incorporated through a further reduction in soil
 281 stiffness used in Equations (9) – (13). Based on data from full-scale pile tests (Figure 7
 282 shows data for piles in sand appropriate for this study after [22]) a simple empirical
 283 relationship can be determined for a reduction factor on elastic pile stiffness as a function of
 284 (normalised) pile displacement:

$$285 \quad g_m = \begin{cases} 1.0 & \frac{y_{pi}}{B} \leq 0.004 \\ 6.40 \times 10^{-2} \left(\frac{y_{pi}}{B} \right)^{-0.5} & \frac{y_{pi}}{B} \geq 0.004 \end{cases} \quad (24)$$

286 3.4 Combined SPI model

287 For use within the sliding block method, i.e. for determining the instantaneous value of
 288 P_i in Equation (3), a direct relationship between P_i and slope slip y_{si} is desirable, so that the
 289 slip computed from the previous step can be used to obtain the current pile resistance force.
 290 This can be achieved by following the following procedure:

- 291 1. Estimate the operative shear modulus within the stable soil (Section 3.3) and use this
 292 to determine G_c , ρ_c and L_c .
- 293 2. Substitute Equation (9) into Equation (7) for the unknown pile displacement y_{pi} .
- 294 3. The resulting (non-linear) closed-form expression can then be used to evaluate P_i
 295 over a fine grid of y_{si} values using the values of G_c , ρ_c and L_c from step (1), and these
 296 values of P_i reduced by p_m to account for the pile spacing.
- 297 4. Values of y_{pi} compatible with the P_i , y_{si} pairs can then be evaluated using either
 298 Equation (7) or Equation (9) and used to determine stiffness multipliers g_m .

299 5. The stiffness G_c is reduced by g_m and reduced values of P_i are evaluated over the
300 same grid of y_{si} values.

301 The result of this procedure is a unique P_i - y_{si} curve which can be used at a particular time
302 step in a sliding block analysis to evaluate the current resistance force based on the current
303 accumulated soil slip from the previous step. This force is then used in Equation (3) to
304 evaluate the current value of k_{hy} for determining slope deformation via Newmark analysis. A
305 flowchart, showing the complete procedure is shown in Figure 8.

306 3.5 Determination of bending moment profile in piles

307 Once the sliding-block analysis has been completed, the variation of P with time will
308 have been determined as an integral part of the analysis. Once this instantaneous load is
309 known, it is relatively simple to estimate the bending moments within the pile as they are
310 proportional to P while the pile remains elastic. Randolph [15], as cited in Fleming et al.
311 [23], present normalised bending moment profiles for partially embedded piles (which,
312 following the previous analogy, apply below the slip plane in this case) for the cases of
313 moment-only loading and shear-only loading. If the pile remains elastic, the principle of
314 superposition can be used to combine the effects of the shear force ($= P_i$) and moment
315 ($= P_i \times 0.33z_{slip}$) acting at the location of the slip plane depth. Above the slip plane (i.e.
316 within the slipping soil) the bending moments are assumed to reduce linearly from the value
317 at the slip plane to zero at the ground surface (consistent with the lateral bearing capacity of
318 the soil increasing linearly with the depth and all of the soil within this zone being at yield).

319 Normalised moment curves ($M_i / P_i L_c$) for different slip plane depths have been created
320 as a function of normalised depth below the slip plane $(z - z_{slip}) / L_c$ and these are shown in
321 Figure 9 for $\rho_c = 1.0$ i.e. for G increasing linearly with depth. As the value of β_i reduces with
322 slip, once the pile has reached its ultimate value of P (soil slip around the pile) there can be
323 further increase in the induced moments due to re-grading.

324 4. Validation of Newmark method for piled slopes against centrifuge data

325 4.1 Centrifuge modelling

326 Dynamic centrifuge testing was conducted using the 3.5 m diameter beam centrifuge
327 and servo-hydraulic earthquake simulator (EQS) at the University of Dundee. The modelling
328 and observations from these tests are described in detail in [10]; only a brief summary is
329 given here. All subsequent properties are reported at prototype scale.

330 The results of six tests from this previously reported programme are utilised herein for
331 validation of the Newmark model, representing identical 1:2 slopes ($\beta_0 \approx 28^\circ$) at 1:50 scale in
332 dry HST95 sand and tested at 50-g. The sand was pluviated in air using a slot pluviator into
333 an Equivalent Shear Beam (ESB) container having flexible walls, the construction of which is
334 described in [24]. The slopes were prepared at a relative density of $D_r = 55 - 60\%$ (the range
335 accounts for the accuracy in being able to measure and replicate D_r), 8 m tall from toe to
336 crest and were underlain by a further 6 m of sand at the same relative density. Table 1
337 shows a summary of the test properties, while the arrangement and instrumentation of the
338 slope models are shown in Figure 10.

339 Where piles were used these all had a square cross-section with $B = 0.5$ and an
340 'elastic' section with a high moment capacity (M_{ult}), fabricated from aluminium alloy as
341 described in [10]. Two of these piles in each test were instrumented to measure bending
342 moments along the length (for comparison to the assumed distributions shown in Figure 9).
343 The bending stiffness of the piles was $EI = 50.4 \text{ MNm}^2$ and $M_{ult} = 3750 \text{ kNm}$

344 The test programme also included the use of two different strong earthquake motions
345 to allow an initial assessment of the model's sensitivity to shaking characteristics. Four tests
346 used a motion recorded at Station TCU072 during the $M_w = 7.6$ Chi-Chi Earthquake in 1999,
347 having a peak ground acceleration (PGA) = 0.41-g, while two tests (AA17 and AA16, see
348 Table 1) used a motion recorded at the Nishi-Akashi recording station in the $M_w = 6.9$ Kobe
349 earthquake in 1995 (PGA = 0.43-g). The characteristics of these motions are described in

350 [1]. In each case four nominally identical motions were applied to each model in sequence
351 to allow the performance in strong aftershocks to be validated.

352 4.2 SPI model for parameters used in the centrifuge tests

353 Figure 11 shows the variation of initial shear modulus (G_0), operative shear modulus
354 (G) calculated using Equation (15) and the measured shear modulus in the free-field from
355 the centrifuge test data. The latter was derived from the time-acceleration histories from
356 instruments 6, 10 and 15 in Figure 10, which were located at the middle of the slope and
357 along the centreline of the container (midway between the two central piles), following the
358 method outlined by Brennan et al. [25]. Figure 12 shows time-shear stress, time-shear strain
359 and a shear stress-shear strain cycle at peak cyclic shear strain from centrifuge test AA14 as
360 an example. Some differences are observed between the operative and measured shear
361 moduli in Figure 11, but the approximate procedure described in Section 3.3 appears to
362 provide a rational basis for making a reasonable estimation of the operative shear modulus
363 for use in the SPI model.

364 Figure 13 shows the P - y_s curves for pile resistance, using soil properties for the
365 centrifuge tests ($\nu'_{pk} = 40^\circ$; $\psi' = 10^\circ$; $\nu^* = 35^\circ$ - see [1]). At $S/B = 7.0$ there is no shadowing
366 effect ($p_m = 1.0$ from Equation (24)) while the curves are reduced in magnitude at $S/B = 4.7$
367 and 3.5. It is clear that once the soil slips by a relatively small amount (10 mm in this case)
368 the pile resistance reaches a maximum value consistent with the unstable soil yielding
369 around the piles. Expressing this displacement in terms of the pile size, $0.015B$, the value is
370 consistent with the lower limit of previous findings for the static case [26, 27] which suggest
371 that the ultimate pile resistance is mobilised within the range $0.015D_{eq}$ to $0.025D_{eq}$.

372 4.3 Analysis procedure

373 To use the sliding block method developed in the previous sections, it is necessary to
374 know the slip plane depth, Z_{slip} . In the centrifuge tests Z_{slip} was not known. However, both
375 crest settlement and bending moment in the piles were measured, so Z_{slip} could be

376 determined by trial and error as the back-calculated value giving a good match
377 simultaneously to both the crest settlements and maximum bending moment magnitude in
378 the first earthquake.

379 Figure 14 shows the effect of pile resistance and geometric re-grading (change in β)
380 on the yield acceleration compared to an unreinforced slope using the first earthquake (EQ1)
381 of test AA01 in each case to determine the effects of the pile reinforcement for an identical
382 input motion. Only the positive (downslope) accelerations have been shown for clarity. It can
383 be seen how the yield acceleration is strongly influenced by the pile resistance for small
384 deformations when the ground motion exceeds the yield acceleration. The pile resistance is
385 mobilised rapidly with slip (consistent with Figure 13). Motion of the slope causes re-grading
386 (geometric hardening) in both the reinforced and unreinforced cases. This is a much more
387 gradual process than the pile resistance mobilisation and the yield acceleration is
388 subsequently seen to increase non-linearly throughout the remainder of the earthquake.

389 4.4 Results

390 The input motion used in the sliding block analyses was the acceleration time history
391 measured at accelerometer No. 8 (Figure 10) which represents the accelerometer at the
392 base of the centrifuge model. This is consistent with the approach for unreinforced slopes
393 presented in [1]. Figure 15 shows a comparison of predicted and measured response for
394 $S/B = 7.0$. The inferred slip plane depth giving this result was $z_{\text{slip}} = 1.75$ m. It should be
395 noted that the slip plane depth for the unreinforced slope is 0.5 m ([1]). Figure 16 shows a
396 similar comparison for $S/B = 4.7$ (for $z_{\text{slip}} = 1.77$ m) and Figure 17, the comparison for $S/B =$
397 3.5 ($z_{\text{slip}} = 1.65$ m).

398 Considering Figures 15-17 together, it can be seen that in general, the new sliding
399 block method slightly under-predicts deformations in the initial earthquake, though this is
400 worst for the widest spacing and the prediction at closer S/B ratios (a more likely case for
401 design to have the most reinforcing effect) becomes significantly better. Deformations in

402 subsequent earthquakes (e.g. strong aftershocks) are generally slightly over-predicted,
403 which for use in whole-life design of a piled slope (with very many earthquakes), would be
404 conservative. The maximum bending moments reach a limiting value in the first earthquake,
405 in each case representing the peak moment associated with the soil in the slipping mass
406 yielding around the pile. The centrifuge test data suggests proportionally small increases in
407 induced moment in subsequent aftershocks. Increases in subsequent earthquakes are also
408 suggested in the sliding block model due to the reducing value of β_i , but these are much
409 smaller in magnitude. The difference be the result of a small amount of rigid body rotation in
410 addition to the pile bending (rigid body rotation is not incorporated into the current
411 implementation of the sliding block model). The effect of localised non-linearity (through g_m)
412 has a modest effect, resulting in slightly larger deformations for the same amount of induced
413 bending moment in the piles. In each case, the yield acceleration can be seen to exhibit the
414 same characteristics as described in Figure 14, namely an initial rapid mobilisation of the pile
415 resistance, followed by subsequent increases due to geometric hardening. It is noticeable
416 that the maximum bending moments in the centrifuge test data in EQ1 have a stepped
417 appearance, initially mobilising half the ultimate resistance during the large acceleration
418 spikes occurring between 10-15 s, before increasing to the ultimate value based on soil yield
419 around the pile. This would be consistent with the SPI model being stiffer than the actual
420 behaviour (i.e. P is mobilised over a smaller amount of deformation in the model) and so
421 there is potentially still some improvement that could subsequently be made to the SPI
422 model. However, given the simplifications and assumptions in the current implementation, it
423 appears to provide consistent and largely accurate predictions of slope and pile response to
424 large deformations over multiple successive earthquakes.

425 Figure 18 shows the bending moment distributions as a function of depth at the end of
426 EQ1 for the instrumented pile cases discussed previously. It can be seen that while the
427 magnitude of the peak bending moment and the moment distribution above the inferred slip
428 plane depth appear to be well predicted, the position of the peak moment and the moments

429 below this depth are under-predicted. However, the shape of the predicted and measured
430 curves are similar. These two observations suggest that the critical length of the piles (L_c) is
431 longer than that predicted using Equation (11). The parameter g_m was incorporated to
432 account for reduction in the operative shear modulus in the near-field (due to pile
433 deformation) compared to the free-field values (Figure 11), but this is shown to only have a
434 modest (though positive) effect on the moments. The zero moment point from the centrifuge
435 data and the increased moments at depth would be consistent with a small amount of rigid
436 body rotation, superimposed onto the pile bending mechanism incorporated within the
437 model. Nonetheless, in each case the magnitude of the peak bending moment is well
438 predicted in each case and so the model would appear to be adequate for use in design
439 (determination of pile size and spacing), so long as the pile is designed to have uniform
440 moment capacity with depth, and this is based on the maximum value.

441 **5. *A priori* determination of Z_{slip}**

442 In the forgoing validation, the sliding block method was used to obtain (simultaneously)
443 good predictions of slope displacements and pile bending moments, allowing the empirical
444 estimation of Z_{slip} . However, for practical use it would be more useful if an *a priori*
445 determination of Z_{slip} could be made, for which it would be necessary to find the optimal
446 position of the slip surface in the piled slope. Here, the Discontinuity Layout Optimisation
447 (DLO) technique was used to achieve this [28]. DLO essentially performs upper-bound
448 plasticity analysis in soils with associative flow, via a virtual work (energy balance) type
449 approach. This approach is common for determining collapse loads of geotechnical systems
450 (e.g. bearing capacity of shallow foundations [29]) but requires the critical failure mechanism
451 to be identified (i.e. the configuration of slip lines forming a mechanism which gives the
452 lowest collapse load or least upper-bound). DLO provides an efficient way of identifying this
453 mechanism from all possible combinations of discontinuities that can be formed by linking
454 regularly spaced nodes across a grid, and allows pseudostatic earthquake accelerations to

455 be accounted for [30]. As in [1], LimitState:GEO, v2.0 software was used to calculate the
 456 most critical (lowest) upper-bound mechanism by DLO for the geometry and properties of
 457 the centrifuge model.

458 To allow soil yield around the piles in what is otherwise a two-dimensional analysis, the
 459 piles were represented as 'engineered elements' [31] which allow relative displacement
 460 between the soil and each node of this element based on the exceedence of a limiting value
 461 of resistance (i.e. the maximum value of P in Figure 13). Three main parameters are
 462 required to define the properties of engineered elements: (i) lateral resistance per unit length
 463 and width to lateral displacement (N); (ii) axial resistance per unit length and width, (T); and
 464 (iii) moment resistance of the element per unit width (pile M_{ult}). A linear variation with depth
 465 was assumed for both lateral and axial resistance:

$$466 \quad T = T_c + T_q \cdot \sigma'_{v0} \quad (25)$$

$$467 \quad N = N_c + N_q \cdot \sigma'_{v0} \quad (26)$$

468 The spacing ratio was taken into account in determining the parameters in Equations (25)
 469 and (26), so that they represent equivalent values per unit length of the slope. As the pile
 470 elements have their tops at the surface of the slope where both resistances are expected to
 471 be zero, $T_c = N_c = 0$. The depth-dependent parameters T_q and N_q are given by:

$$472 \quad T_q = \frac{4 \cdot B \cdot (2K_o) \cdot \tan \delta'}{S} \quad (27)$$

$$473 \quad N_q = \frac{K_p^2}{(S/B)} \quad (28)$$

474 where $K_p = (1 + \sin \nu') / (1 - \sin \nu')$ is the passive earth pressure coefficient and δ' is the
 475 interface friction angle between the pile and the soil (based on interface shear test data
 476 reported in [10]). T_q therefore represents the axial shaft capacity for a square pile in sand,
 477 while N_q is a lateral bearing capacity factor, based on [32]. The moment capacity of the
 478 piles, divided by the pile spacing, was used in determining the value of M_{ult} .

479 While the strength of the soil over a wide strain range was approximated by u^* in the
480 sliding block analyses, for determining the initial position of the yield surface, the peak
481 friction angle must strictly be used. For stability problems in cohesionless soils it is important
482 to model the true variation of u'_{pk} with depth (where the strength reduces with increased
483 depth and confining stress due to dilation suppression [33]), to avoid the trivial solution of a
484 failure mechanism forming along the surface of the slope. This was modelled by dividing the
485 soil into multiple 0.5 m thick layers over the top 8 m of soil such that each layer can be
486 assigned an independent angle of friction. Figure 19 shows the variation of u'_{pk} used in the
487 DLO analyses based on the results of direct shear tests of the sand used in the centrifuge
488 tests, reported in [1].

489 The value of z_{slip} predicted by DLO was 1.50 m (insensitive to S/B for the parameters
490 used) for the piled slope cases. This is very close to the values of between 1.65 – 1.77 m
491 inferred from the centrifuge test results for the simulations using the Chi-Chi input motion
492 and the value of 1.45 m inferred for test AA16 (Kobe motion) and would suggest that DLO
493 can be used to estimate the required z_{slip} for class A predictions. However, this depends on
494 the sensitivity of the Newmark analysis to this parameter. The centrifuge tests were
495 therefore reanalysed using the sliding block model with the value of z_{slip} predicted from DLO
496 and the results (in terms of prediction of crest settlement and M_{max}) are shown in Figure 20
497 (filled markers) along with the results using back-calculated z_{slip} values for comparison
498 (hollow markers). Using the DLO value of z_{slip} , there is a general increase in the
499 displacements predicted but a significant reduction in M_{max} . The predictions also become
500 worse with further strong shaking, but are very good in EQ1. Over-prediction of
501 displacements will generally result in a more conservative design for a given tolerable
502 amount of slope deformation. Under-prediction of bending moments suggests that a
503 substantial factor of safety should be applied if the calculated moments are to be used to
504 size/detail the piles. In this case, based on the data in Figure 20, a factor of safety of 2.0 is
505 indicated.

506 6. Conclusions

507 The modified Newmark procedure developed by Al-defae et al., [1] for predicting slip in
508 unreinforced cohesionless slopes including strain-induced geometric hardening (slope re-
509 grading) has here been modified to be applicable to pile–reinforced slopes (incorporating
510 strain-dependent pile resistance) to allow estimation of permanent seismic deformation in
511 piled slopes. This is achieved through modifying the yield acceleration at each time step by
512 incorporating mobilised pile resistance forces consistent with the current amount of relative
513 soil-pile movement. This simplified **combined** model needs only relatively basic information
514 about the soil (u' , γ , ν , G_0 , u , c'), slope geometry (β , H , L), pile properties/layout (B , EI , S ,
515 plus M_{ult} for checking capacity is not exceeded) and earthquake (a time history and dynamic
516 amplification factor for estimating a_{max}), and an estimated slip plane depth (z_{slip}). A
517 procedure for estimating z_{slip} via an optimised upper-bound plasticity analysis (here
518 conducted using Discontinuity Layout Optimisation, DLO) was also proposed.

519 The model was validated against a database of centrifuge test results having different
520 pile-to-pile spacing and earthquake excitations in cohesionless soil. The permanent slope
521 deformations and maximum induced bending moments (M_{max}) were predicted extremely
522 closely for first earthquake conditions using back-calculated values of z_{slip} . Using the DLO
523 procedure to estimate this parameter resulted in similarly good deformation estimates, but
524 under-prediction of M_{max} due to the high sensitivity of M_{max} to z_{slip} . This implies that there is
525 scope to develop the z_{slip} predictions further. The method can also be applied to subsequent
526 strong shaking (aftershocks), but the predictions, while reasonable, become poorer as
527 greater numbers of subsequent earthquakes are applied (generally over-estimating crest
528 deformation and under-estimating M_{max}).

529 The model will be useful in seismic design for determining appropriate pile layouts and
530 sizing/detailing to meet a prescribed amount of slope deformation at the crest while ensuring
531 that the piles remain elastic. This will provide a useful screening tool for identifying

532 promising configurations for further, more detailed numerical (Finite Element) modelling
533 which can fully verify dynamic behaviour.

534

535 **Acknowledgements**

536 The authors would like to express their sincere gratitude to Mark Truswell and Colin
537 Stark at the University of Dundee for their assistance in performing the centrifuge tests. The
538 first author would also like to acknowledge the financial support of his PhD studies from the
539 Ministry of Higher Education and Scientific Research (MOHESR) of the Republic of Iraq.

540

541 **References**

542 [1] Al-Defae, A.H., Caucis, K. and Knappett, J.A. Aftershocks and the whole-life seismic
543 performance of granular slopes. *Géotechnique* 2013. **63**(14):1230-1244.

544 [2] Liang, R.Y. Drilled shaft foundations of noise barrier walls and slope stabilisation. Ohio
545 Department of Transportation and the U.S. Department of Transportation 2002,
546 Federal Highway Administration and The University of Akron, Akron, Ohio, 2002,
547 Report no. 44325-3905.

548 [3] Wang, W. L., Yen, B. C. Soil arching in slopes. *Journal of Geotechnical and*
549 *Geoenvironmental Engineering* 1974: **105** (GT4): pp. 493-496.

550 [4] Ito, A.T. & Matsui, T. Method of estimate lateral forces acting on stabilising piles.
551 Japanese Society of Soil Mechanics and Foundation Engineering 1975: **15**(4): 43-59.

552 [5] Ito, T., Matsui, T. and Hong, W.P. Extended design method for multi-row stabilising piles
553 against landslides. *Journal of Soil and Foundation* 1982: **22**(1): 1-13.

554 [6] Hassiotis, S., Chameau, J.L. & Guanaratne, M. Design method for stabilisation of slope
555 with piles. *Journal of Geotechnical and Geoenvironmental Engineering*, ASCE 1997:
556 **123**(4): 314-323.

557 [7] Kourkoulis, R., Gelagoti, E., Anastasopoulos, I. and Gazetas, G. Stabilisation of
558 seismically unstable slopes using piles: Parametric Analysis. 5th International
559 Conference on Earthquake Geotechnical Engineering, Santiago, Chile, 2011, Vol.1.

560 [8] Newmark, N.M. Effect of earthquakes on dams and embankments. *Géotechnique* 1965:
561 **15**(2): 139-159.

- 562 [9] Matasovic, N., Kavazanjian, E. and YAN, L. Newmark deformation analysis with
563 degrading yield acceleration. *Proceeding of Geosynthetics. Vol. 2, Long Beach,*
564 *California, USA, March 1997, pp 989-1000.*
- 565 [10] Al-Defae, A.H. and Knappett, J.A. Centrifuge modelling of the seismic performance of
566 pile-reinforced slopes. *Journal of Geotechnical and Geoenvironmental engineering,*
567 *ASCE 2014, (In press).*
- 568 [11] Michalowski, R.L., and Shi, L. Bearing capacity of footings over two-layer foundation
569 soils. *Journal of Geotechnical Engineering* 1995: **121**(5): 421–428.
- 570 [12] Drescher, A. and Detournay, E. Limit load in translational failure mechanisms for
571 associative and non-associative materials. *Géotechnique* 1993: **43**(3): 443–456.
- 572 [13] O'Neill, M.W., and Murchison J.M. An evaluation of p-y relationships in sand. A Report
573 to the American Petroleum Institute, PRAC 82-41-1, the University of Houston-
574 University Park, Houston, Texas, 1993.
- 575 [14] American Petroleum Institute, API. Recommended practice for planning, designing, and
576 constructing fixed offshore platforms. API Recommended Practice 2A 2000 (RP-2A-
577 WSD), 21 Edition.
- 578 [15] Randolph, M.F. The response of flexible piles to lateral loading. *Géotechnique* 1981:
579 **31**(2): 247-259.
- 580 [16] Hardin, B.O. and Drnevich, V.P. Shear modulus and damping in soils: Design Equation
581 and Curves. *Journal of Soil Mechanics and Foundation Engineering Division* 1972:
582 **98**(SM7):667-692.
- 583 [17] Seed, H.B., and Idriss, I.M. Simplified procedure for evaluating soil liquefaction
584 potential. *Journal of Soil Mechanics and Foundation Division* 1971: **97** (9): 1249–1273.
- 585 [18] Idriss, I.M. An update to the Seed-Idriss simplified procedure for evaluating liquefaction
586 potential. In *Proceedings, TRB Workshop on New Approaches to Liquefaction, FHWA-*
587 *RD-99- 165, FHWA, Washington, D.C, 1999.*
- 588 [19] Pradel D. Procedure to evaluate earthquake-induced settlements in dry sandy soils.
589 *Journal of Geotechnical & Geoenvironmental Engineering* 1998: **124** (4): 364-368.
- 590 [20] Hayward, T., Lees, A., Powrie, W. & Smethurst. Centrifuge modelling of a cutting slope
591 stabilised by discrete piles. TRL471 report 2000, Transport Research Laboratory,
592 Berkshire, UK.
- 593 [21] Poulos, H.G. and Davis, E.H. (1980). *Pile foundation analysis and Design.* John Wiley
594 & Sons Inc., New York.

- 595 [22] Alizadeh, M. and Davisson, M.T. (1970). Lateral load tests on piles – Arkansas River
596 Project. Journal of the Soil Mechanics & Foundations Division, ASCE, 96(SM5): 1583-
597 1604.
- 598 [23] Fleming, W.G. K., Weltman, A.J., Randolph, M.F. and Elson, W.K.,. Piling engineering.
599 3rd Edition. Halsted Press, New York, NY100116, USA, 2009.
- 600 [24] Bertalot, D. Behaviour of shallow foundations on layered soil deposits containing loose
601 saturated sands during earthquakes. PhD Thesis, University of Dundee, UK, 2013.
- 602 [25] Brennan, A.J., Thusyanthan, N.I. and Madabhushi, S.P.G. Evaluation of shear modulus
603 and damping in dynamic centrifuge tests. Journal of Geotechnical and
604 Geoenvironmental Engineering 2005: **131**(12): 1488-1497.
- 605 [26] Pan, J., Goh, A., Wong, K. and Teh, C. Ultimate soil pressure for piles subjected to
606 lateral soil movement. Journal of Geotechnical and Geoenvironmental Engineering
607 Division 2002: **128**(6): 530-535.
- 608 [27] Bransby, M.F. & Springman, S. Selection of load-transfer functions for passive lateral
609 loading of pile groups. Journal of Computers and Geotechnics 1999: **24**(3): 155-184.
- 610 [28] Smith, C.C. and Gilbert, M. Application of discontinuity layout optimization to plane
611 plasticity problems. Proc. Royal Soc 2007 A: Mathematical, Physical and Engineering
612 Sciences, 463 (2086), October: 2461-2484.
- 613 [29] Knappett, J.A. and Craig, R.F. Craig's Soil Mechanics (8th Edition), Spon Press,
614 Abingdon, UK, 2012.
- 615 [30] Smith, C.C. and Cubrinovski, M. Pseudo-static limit analysis by discontinuity layout
616 optimization: Application to seismic analysis of retaining walls. Soil Dynamics and
617 Earthquake Engineering 2011: **31**(10): 1311-1323.
- 618 [31] Clarke, S.D., Gilbert, M. and Smith, C.C. Modelling discrete soil reinforcement in
619 numerical limit analysis. Canadian Geotechnical Journal: **50**(7): 705-715.
- 620 [32] Fleming, W.G.K., Weltman, A.J., Randolph, M.F. and Elson, K. Piling Engineering (3rd
621 Edition), Taylor and Francis, Abingdon, UK, 2009.
- 622 [33] Bolton, M.D. The strength and dilatancy of sands. Geotechnique 1986: **36**(1):65-78.
623

624 **Notation**

625 Roman:

626	A	Monotonic/cyclic loading factor for P-y curve
627	a	Shear strain constant
628	a_{max}	Peak acceleration at ground surface
629	B	Pile width
630	b	Shear strain constant
631	c'	Cohesion intercept
632	$C_{1,2}$	Lateral pile resistance constants
633	d	Incremental slope-parallel slip
634	D_{eq}	Equivalent diameter of a circular pile
635	D_r	Relative density
636	e	Natural void ratio
637	E_p	Pile Young's Modulus for equivalent solid circular section
638	EI	Bending stiffness (pile)
639	G	Shear modulus
640	G_o	Small strain modulus
641	G_c	Shear modulus associated with critical length
642	\bar{G}_{Lc}	Median value of operative shear modulus over the critical length
643	g	Acceleration due to gravity (= 9.81 m/s ²)
644	g_m	Stiffness reduction factor for local non-linearity in stable soil
645	H	Slope height above toe
646	k	Subgrade reaction modulus
647	k_h	Pseudo-static seismic horizontal acceleration (g)
648	k_{hy}	Yield acceleration (g)
649	K_0	Lateral earth pressure coefficient (at rest)
650	K_p	Passive lateral earth pressure coefficient

651	L	Length along slip plane
652	L_c	Critical length of pile (below slip plane)
653	M	Bending moment
654	M_{\max}	Maximum induced pile bending moment
655	M_{ult}	Pile bending moment capacity
656	M_w	Moment magnitude
657	$N_{c,q}$	Pile lateral resistance per unit shaft area (constant, depth dependent)
658	p_a	Atmospheric pressure (= 100 kPa)
659	p_m	P-multiplier (pile shadowing effect)
660	p_u	Ultimate lateral soil-pile resistance (per metre length of pile)
661	p'_0	Initial mean confining stress
662	P	Pile-soil resistance force (single pile)
663	r_d	Stress reduction factor
664	S	Pile centre-to-centre spacing
665	$T_{c,q}$	Pile axial resistance per unit shaft area (constant, depth dependent)
666	u	Pore water pressure
667	y_p	Pile lateral deformation (at $0.67z_{\text{slip}}$ below soil surface)
668	y_s	Cumulative soil slip
669	z	Depth below ground surface
670	z_{slip}	Depth of slip plane
671	<u>Greek:</u>	
672	$\alpha_{1,2}$	Stress reduction coefficients
673	β	Slope angle
674	β_0	Initial slope angle (pre-earthquake)
675	γ	Soil unit weight
676	γ'	Effective (buoyant) unit weight
677	γ_w	Unit weight of water (= 9.81 kN/m ³)

678	δ'	Interface friction angle
679	ε_s	Shear strain
680	$\varepsilon_{s,cyc}$	Cyclic shear strain
681	φ'	Effective angle of friction
682	φ^*	Angle of friction (accounting for non-associativity)
683	φ'_{cs}	Critical state angle of friction
684	φ'_{pk}	(Secant) Peak angle of friction
685	ν	Poisson ratio (soil)
686	ρ_c	Homogeneity factor (shear modulus variation with depth)
687	σ_{v0}	Total overburden (vertical) stress
688	σ'_{v0}	Effective overburden (vertical) stress
689	σ'	Normal effective stress
690	$\tau_{applied}$	Applied shear stress
691	τ_{av}	RMS average cyclic shear stress
692	τ_{ult}	Soil shear strength
693	ψ'	Effective angle of dilation

Table 1: Summary of centrifuge test database for model validation

Test ID	D_r (%)	S/B	Input motion	No. of earthquakes
AA01	56	Unreinforced	Chi-Chi	4
AA13	60	7.0	Chi-Chi	4
AA14	57	4.7	Chi-Chi	4
AA15	59	3.5	Chi-Chi	4
AA17	59	Unreinforced	Kobe	4
AA16	57	4.7	Kobe	4

Figures Captions

Figure 1: Slip mechanism in pile-reinforced slope; (a) overall configuration; (b) forces acting on a pile-stabilised slipping soil element.

Figure 2: Simplified model for geometric hardening (slope re-grading) for a slope suffering translational slip (after [1]).

Figure 3: Modelling approach for soil-pile interaction (SPI).

Figure 4: P-y coefficients as a function of friction angle (after [14]).

Figure 5: Stable soil interaction and definition of shear modulus within stable soil.

Figure 6: Relationship between p-multiplier and normalised pile spacing (pile shadowing effect).

Figure 7: Relationship between g_m and pile deformation y_{pi} (effect of non-linearity in stable soil)

Figure 8: Flow chart summarising analysis procedure.

Figure 9: Normalised bending moment curves for piles resisting an infinite slip.

Figure 10: Centrifuge model layout, with instrumented elastic piles shown, dimensions in m prototype scale (mm model scale in brackets).

Figure 11: Comparison of predicted operative shear modulus with depth and centrifuge test observations.

Figure 12: Shear stress, shear strain and shear modulus in test AA14, EQ1: (a) at 2.75 m depth, (b) at 4.50 m depth, (c) at 6.25 m depth.

Figure 13: Calculated SPI curves for centrifuge test conditions.

Figure 14: Effect of pile resistance mobilisation and geometric hardening on slope behaviour; (a) crest settlement; (b) development of yield acceleration.

Figure 15: Validation for test AA13 ($S/B = 7.0$): (a) Predicted and measured crest settlement; (b) Predicted and measured maximum moment (M_{max}); (c) variation of yield acceleration and input motion.

Figure 16: Validation for test AA14 ($S/B = 4.7$): (a) Predicted and measured crest settlement; (b) Predicted and measured maximum moment (M_{max}); (c) variation of yield acceleration and input motion.

Figure 17: Validation for test AA15 ($S/B = 3.5$): (a) Predicted and measured crest settlement; (b) Predicted and measured maximum moment (M_{max}); (c) variation of yield acceleration and input motion.

Figure 18: Predicted and measured bending moments along piles, end of EQ1: (a) Test AA13; (b) Test AA14; (c) Test AA15.

Figure 19: Peak friction angle used to determine initial position of slip surface.

Figure 20: Effect of using DLO-predicted slip plane depth on prediction of slope deformation and maximum pile bending moments.

Figure 1
[Click here to download high resolution image](#)

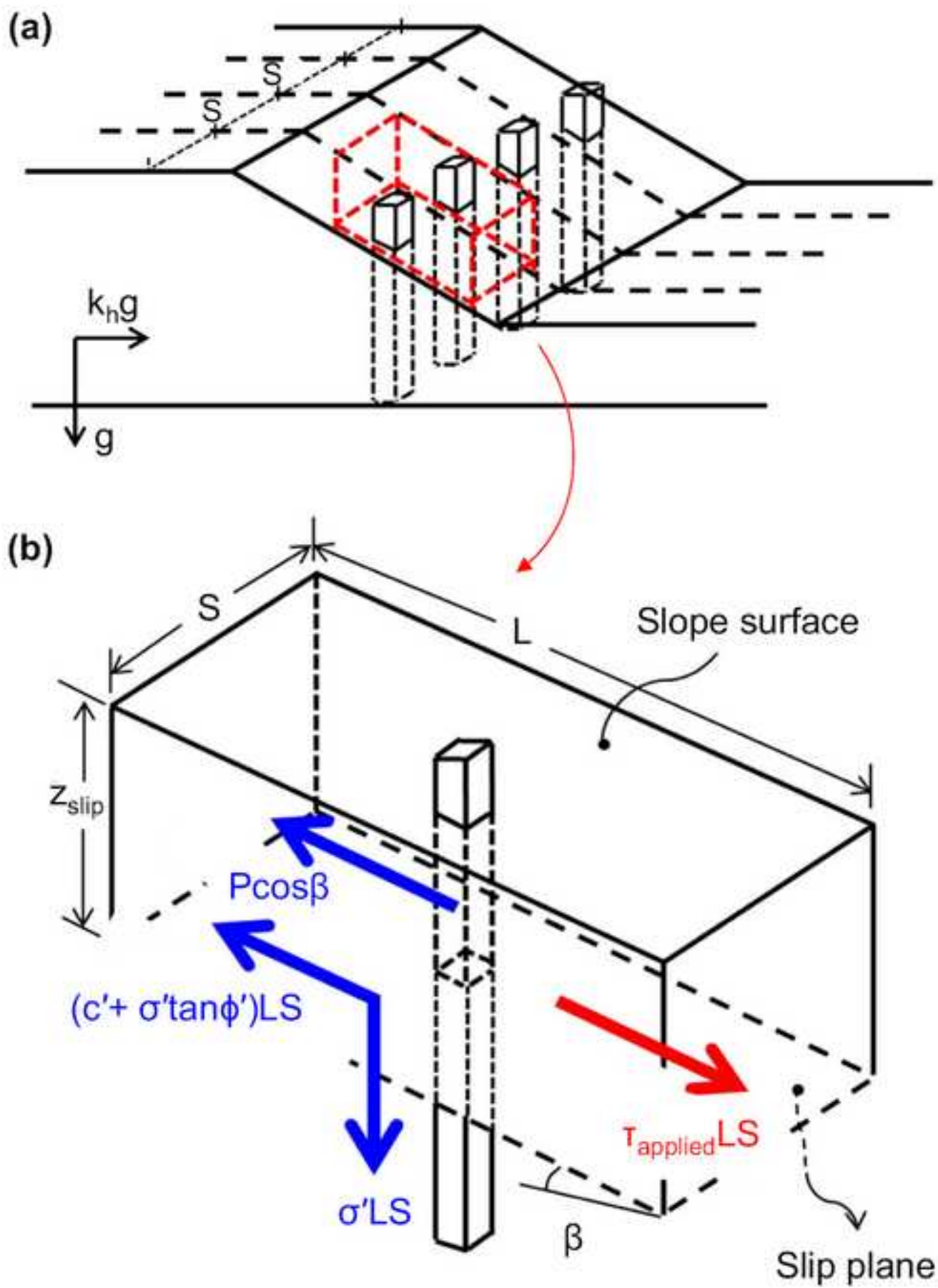
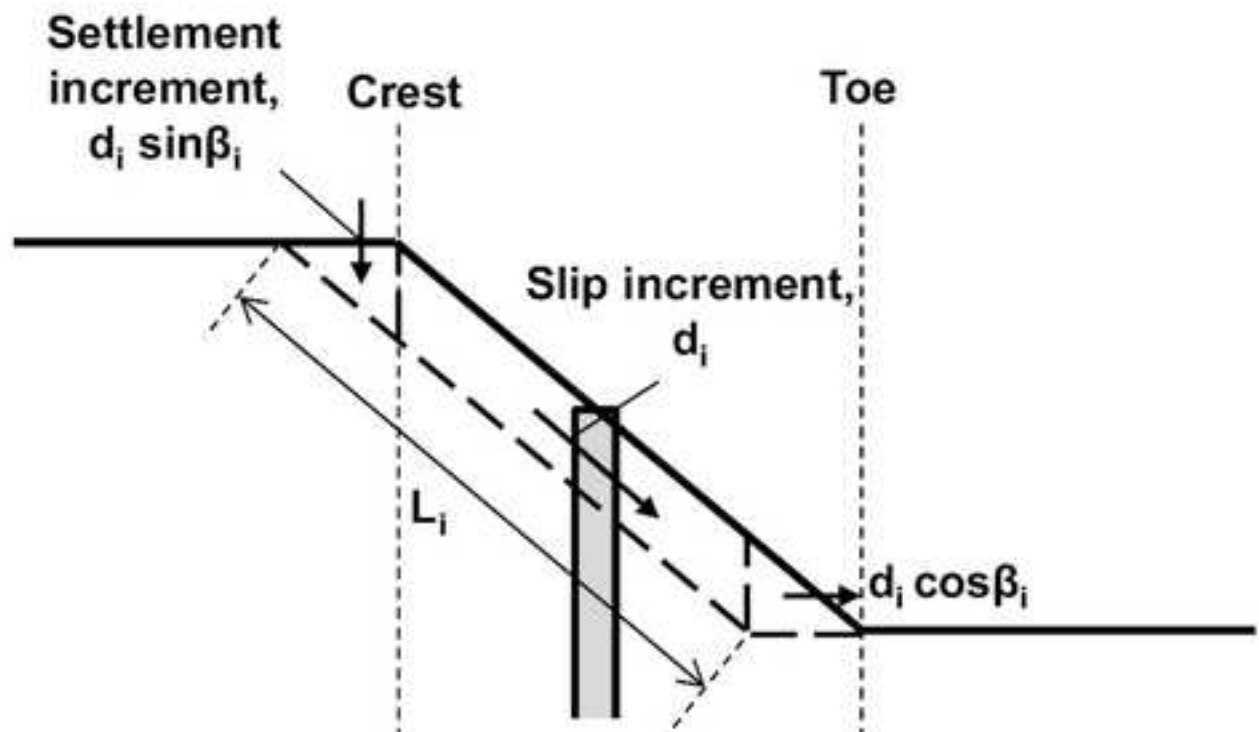


Figure 2
[Click here to download high resolution image](#)

Step i_- :



Step i_+ :

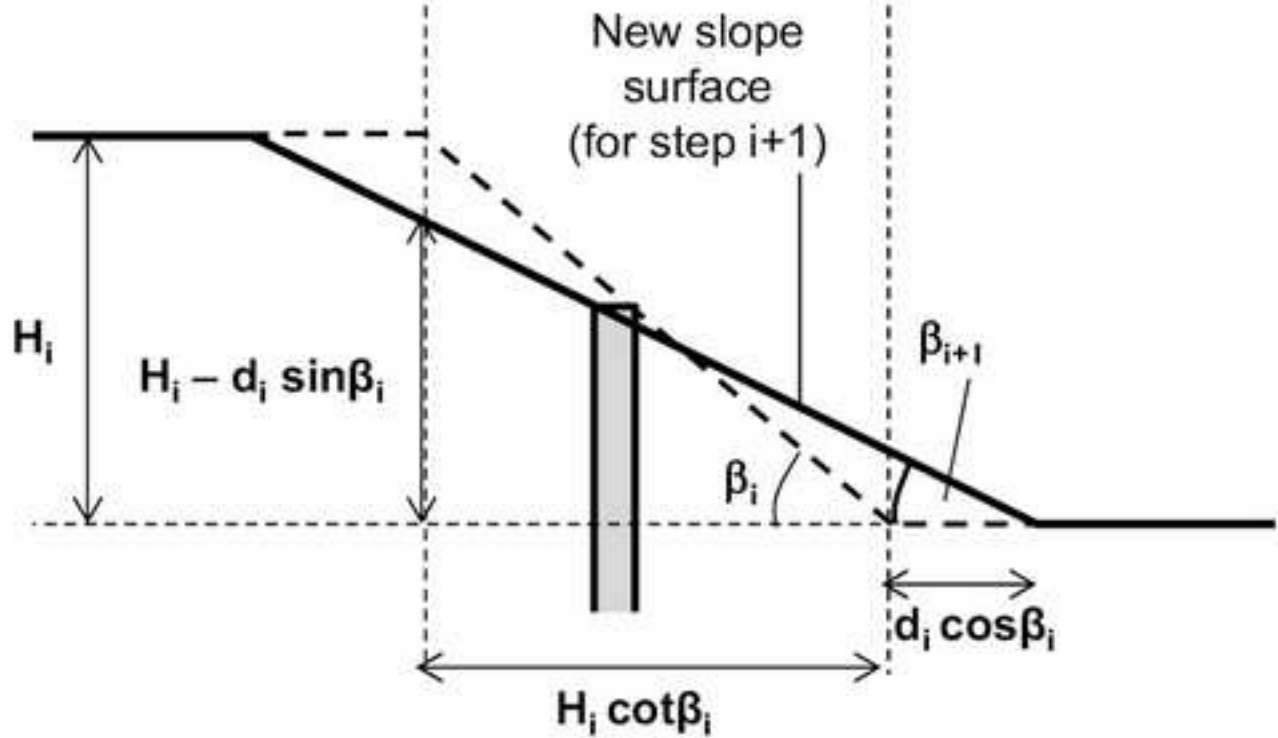


Figure 3
[Click here to download high resolution image](#)

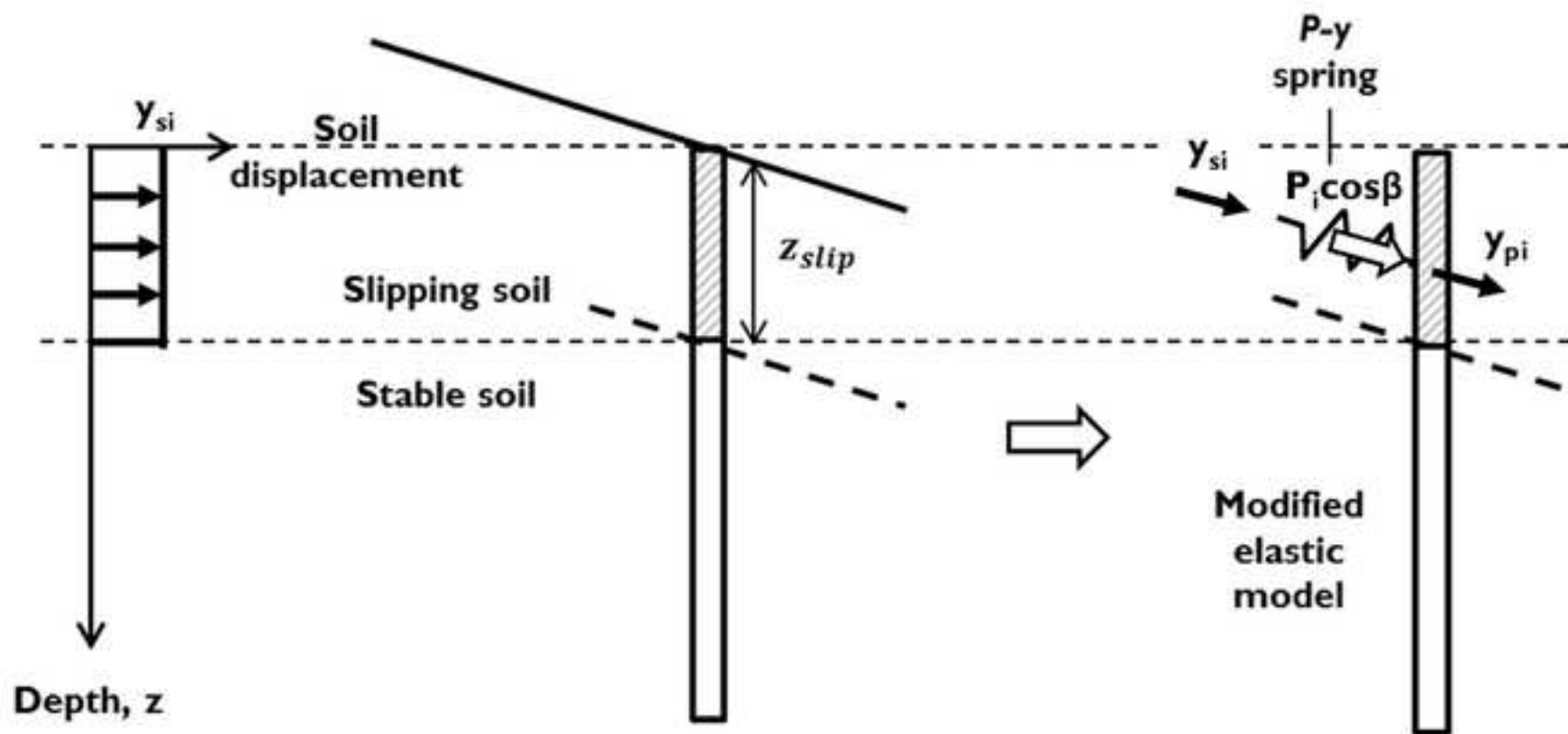


Figure 4
[Click here to download high resolution image](#)

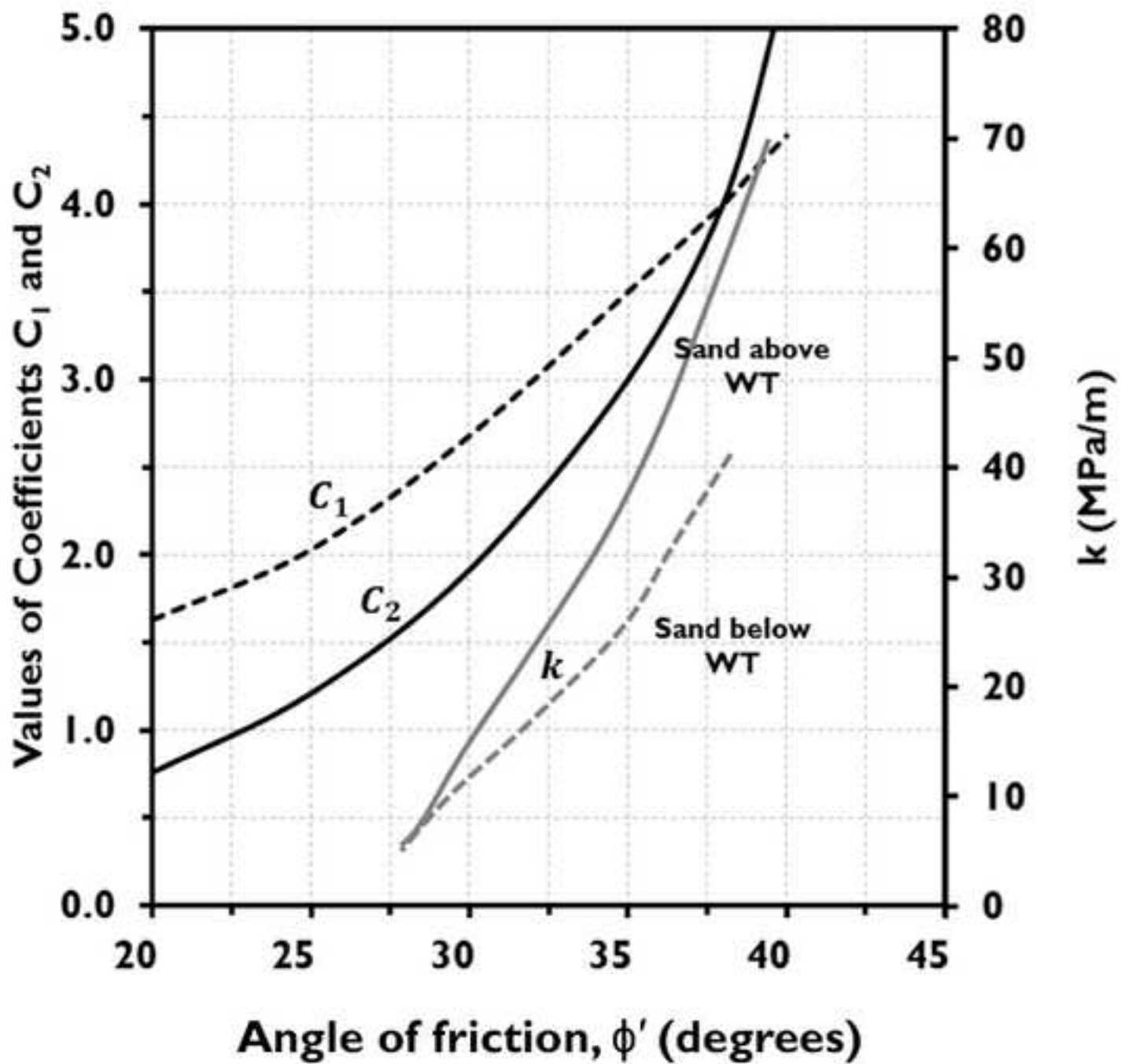


Figure 5
[Click here to download high resolution image](#)

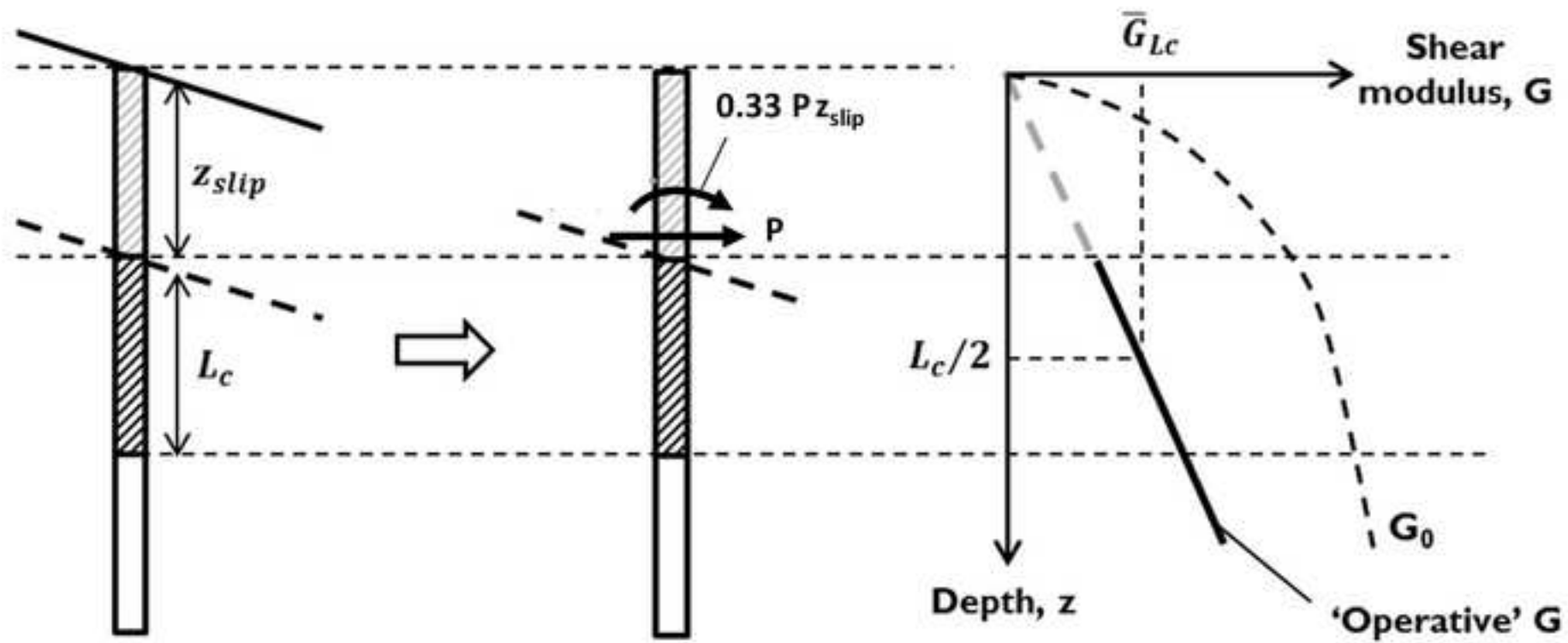


Figure 6
[Click here to download high resolution image](#)

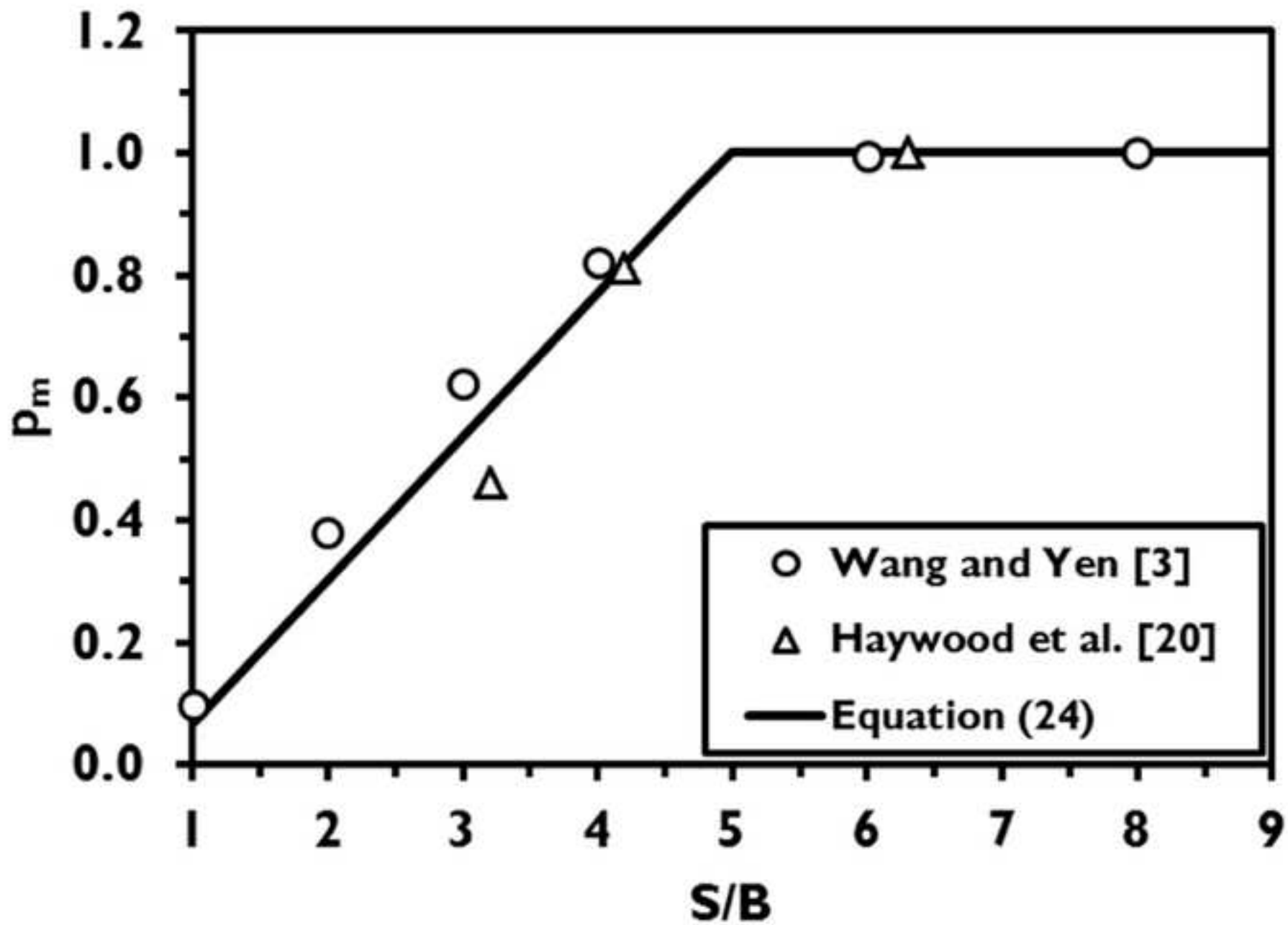


Figure 7
[Click here to download high resolution image](#)

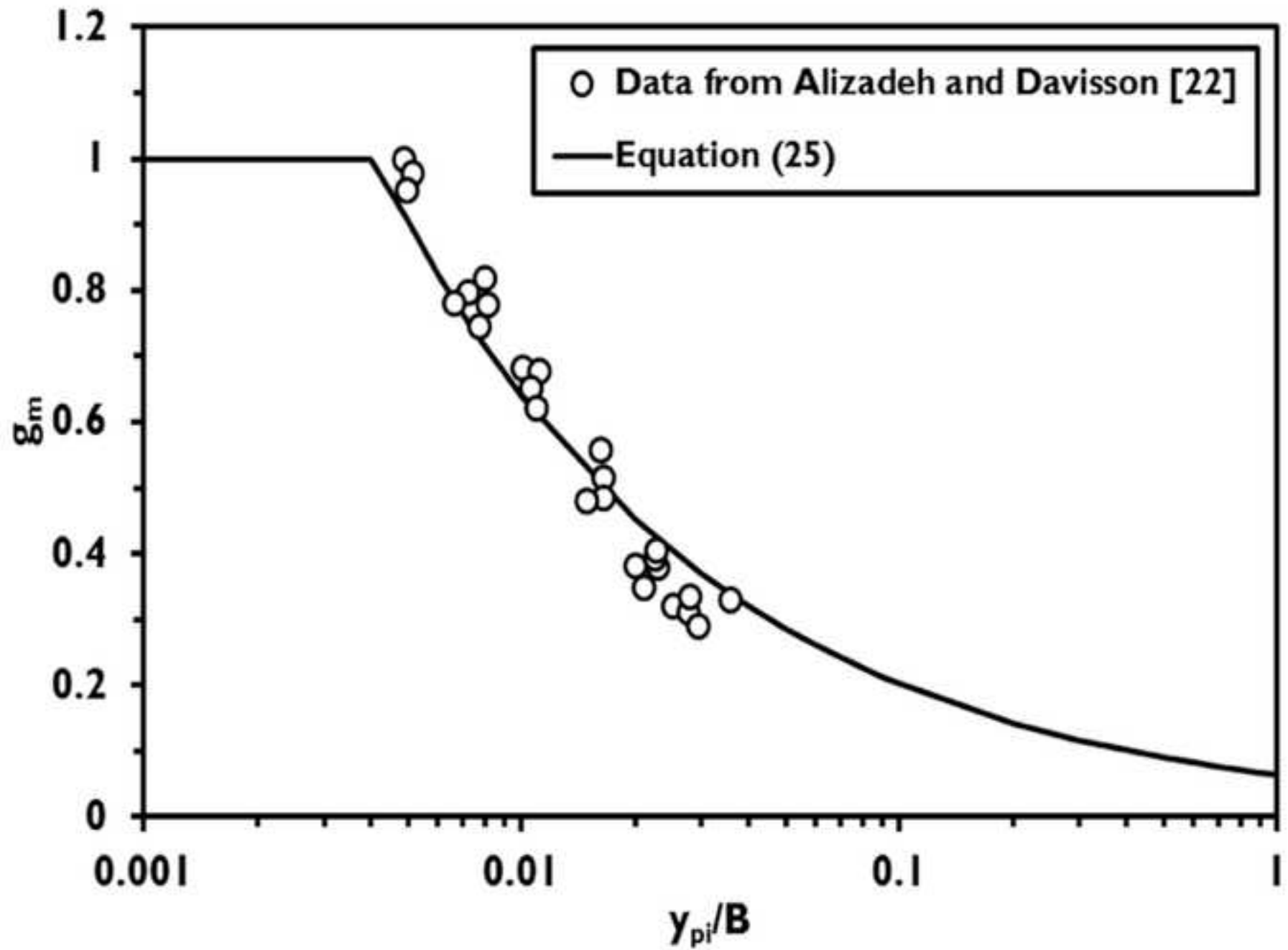


Figure 8
[Click here to download high resolution image](#)

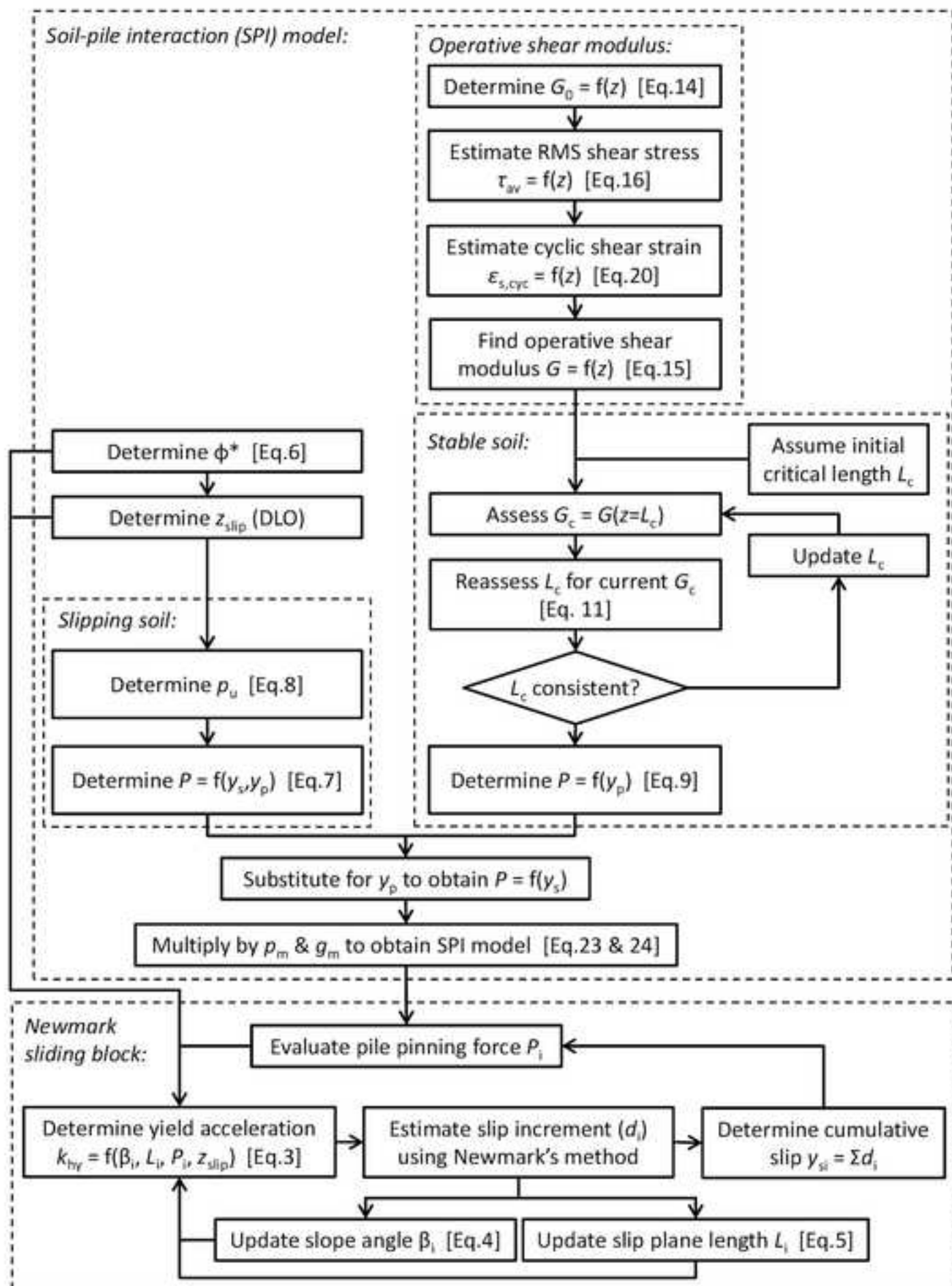


Figure 9
[Click here to download high resolution image](#)

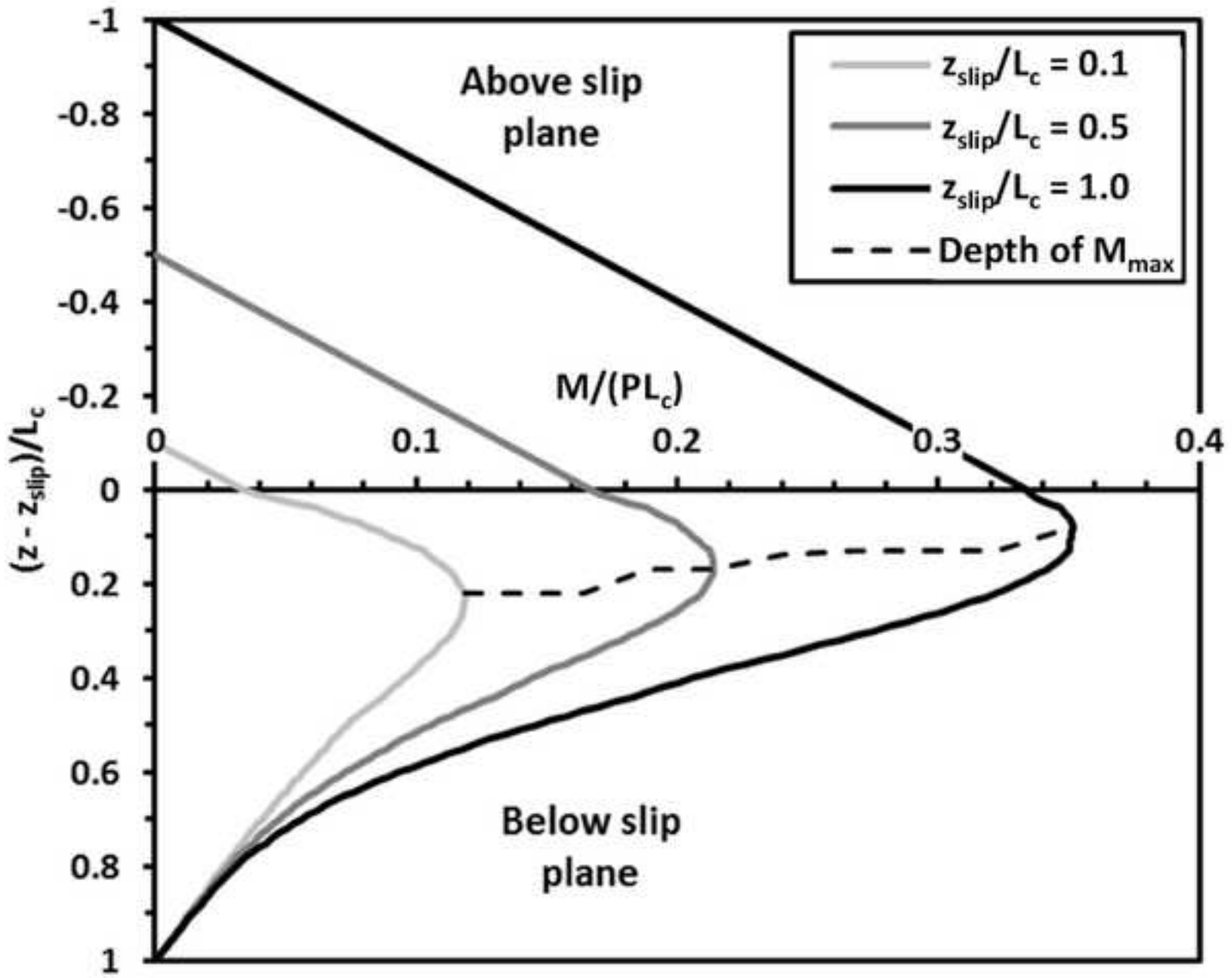


Figure 11
[Click here to download high resolution image](#)

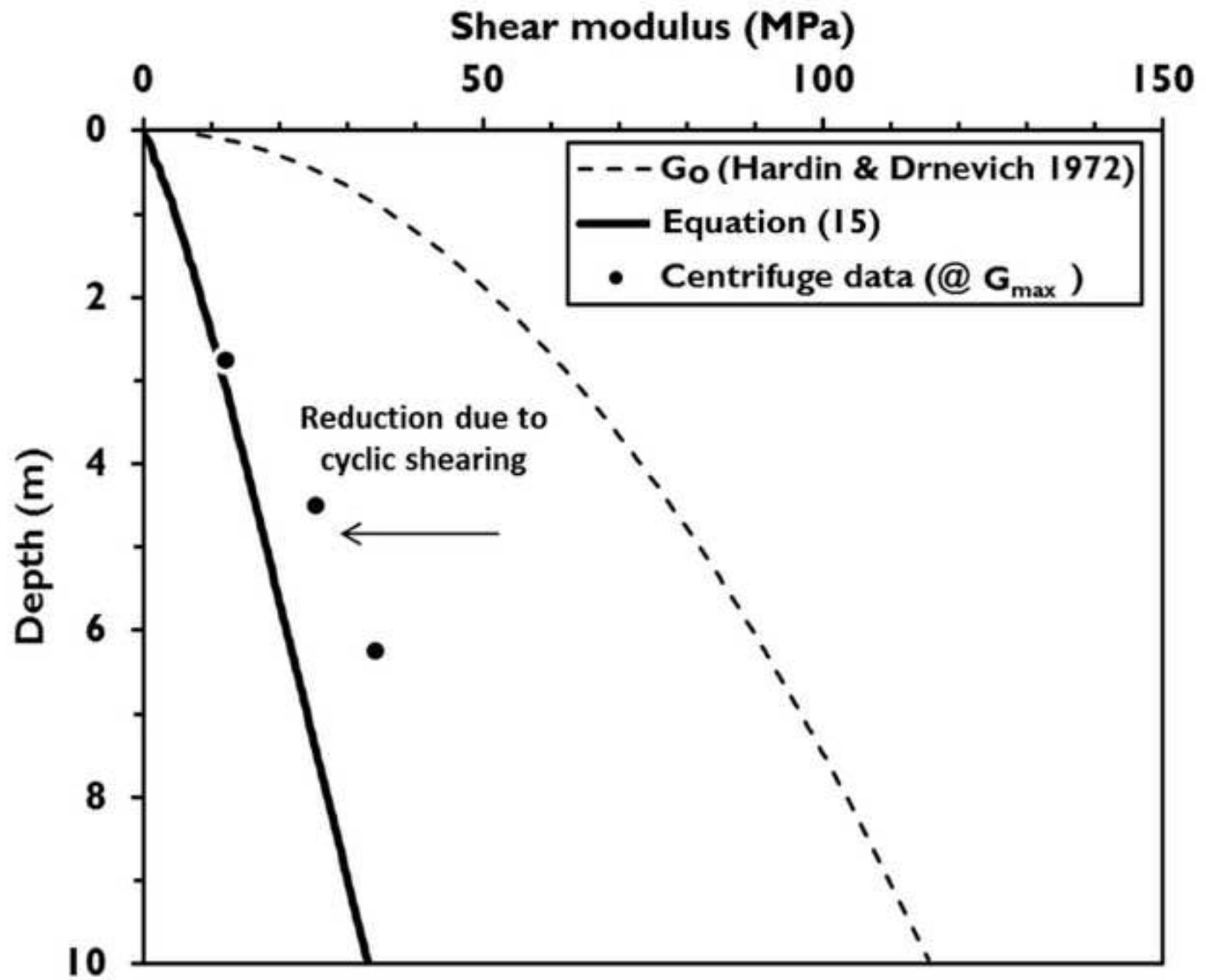


Figure 12
[Click here to download high resolution image](#)

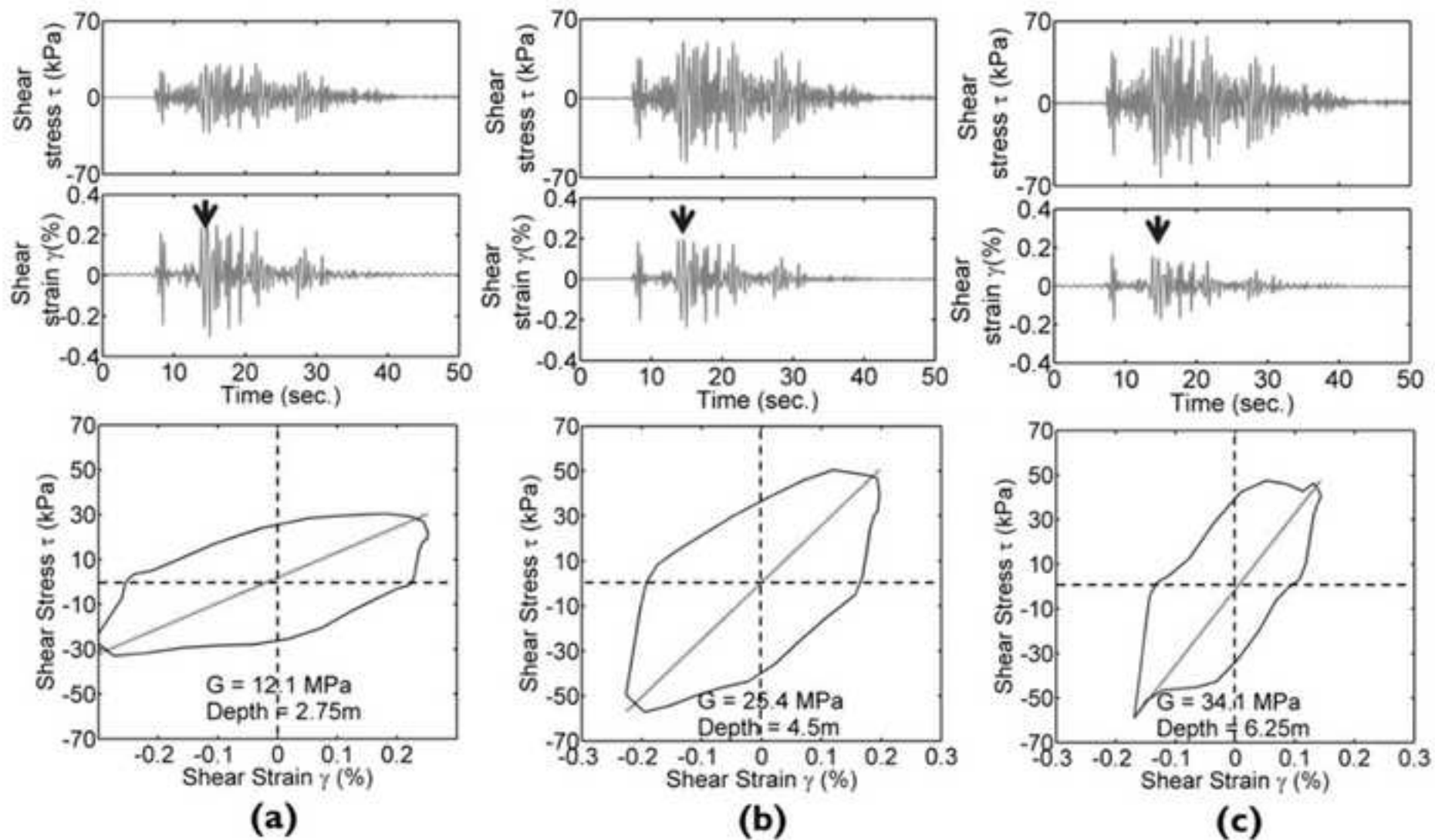


Figure 13
[Click here to download high resolution image](#)

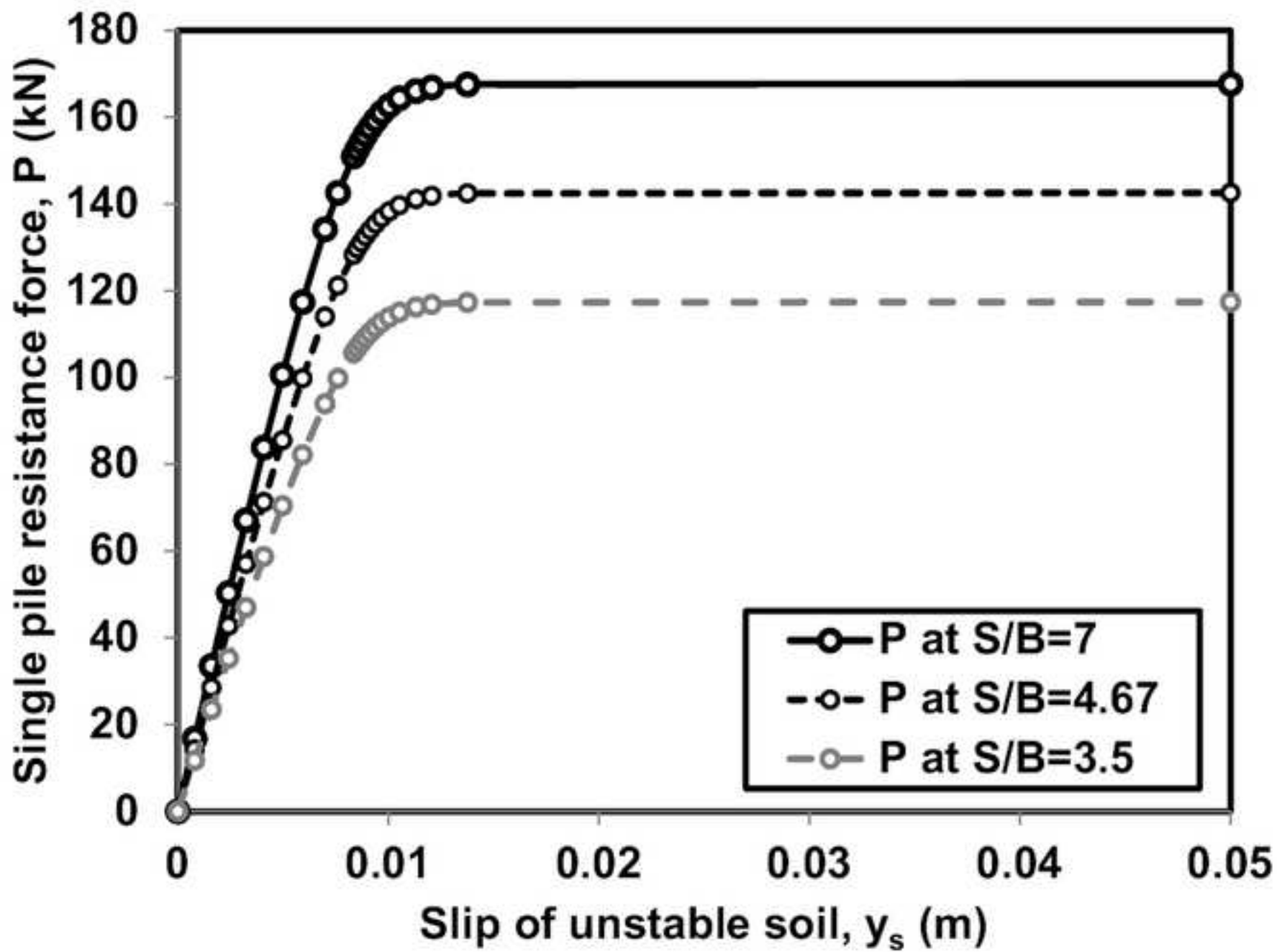


Figure 14

[Click here to download high resolution image](#)

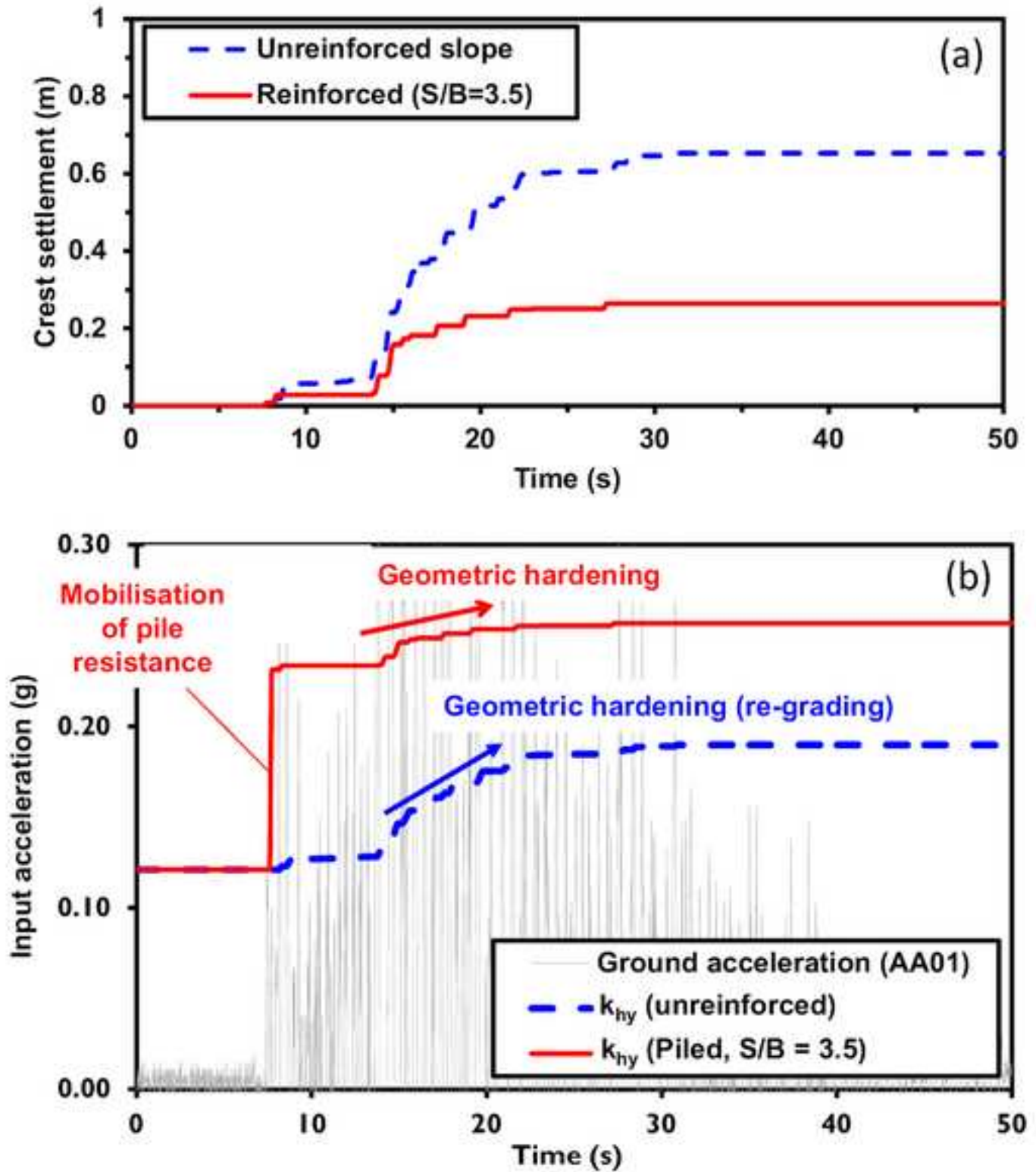


Figure 15

[Click here to download high resolution image](#)

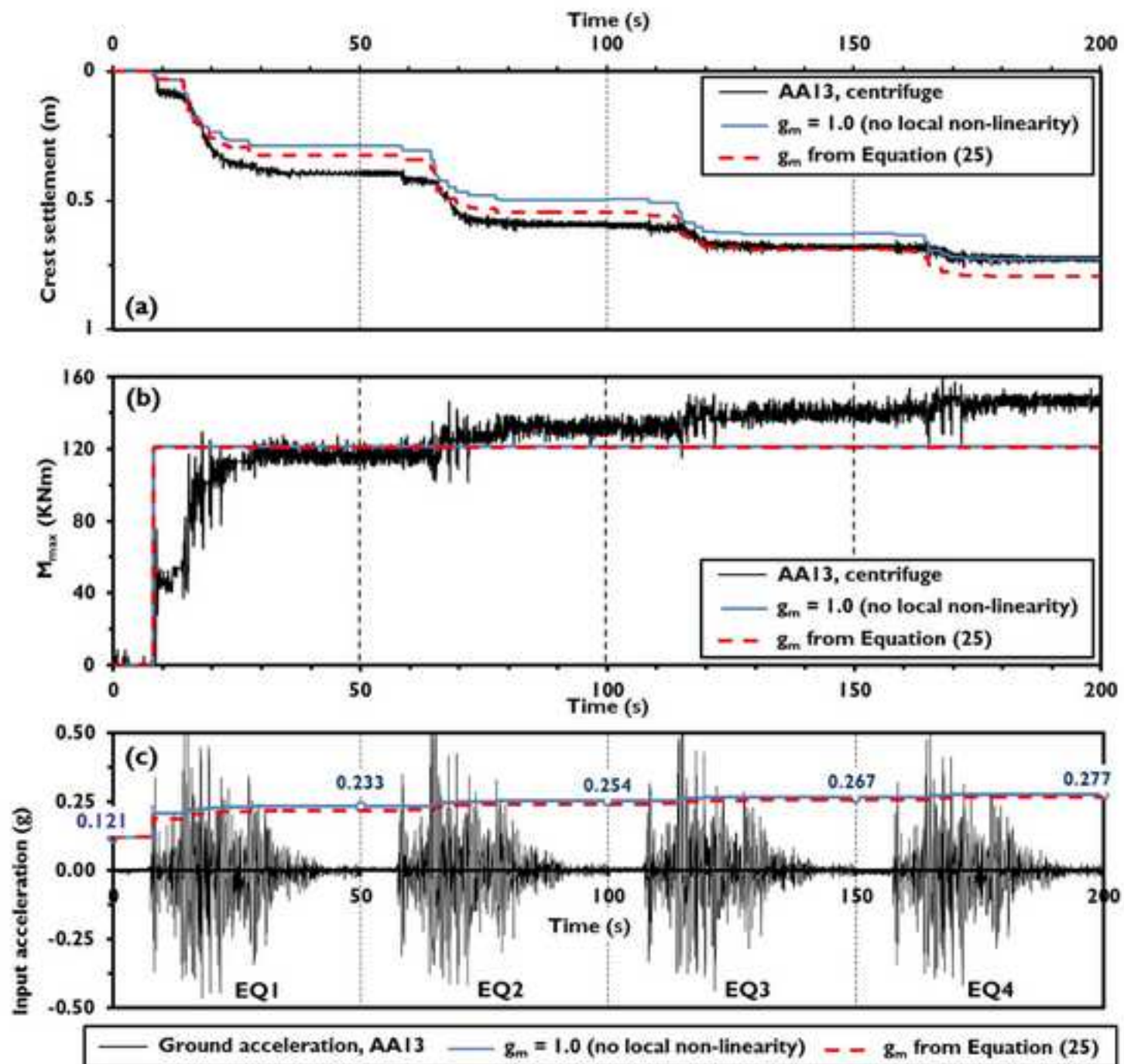


Figure 16
[Click here to download high resolution image](#)

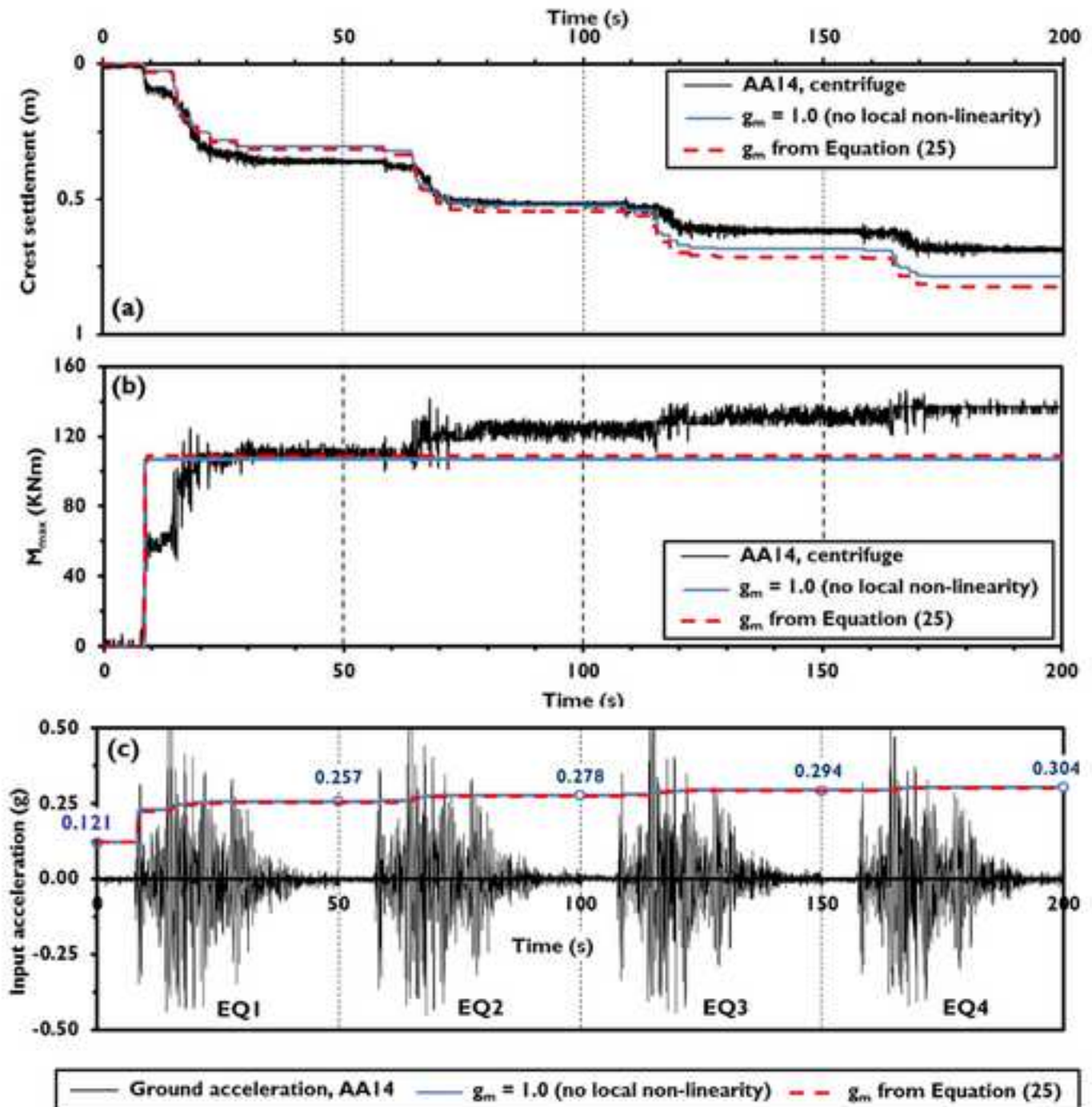


Figure 17

[Click here to download high resolution image](#)

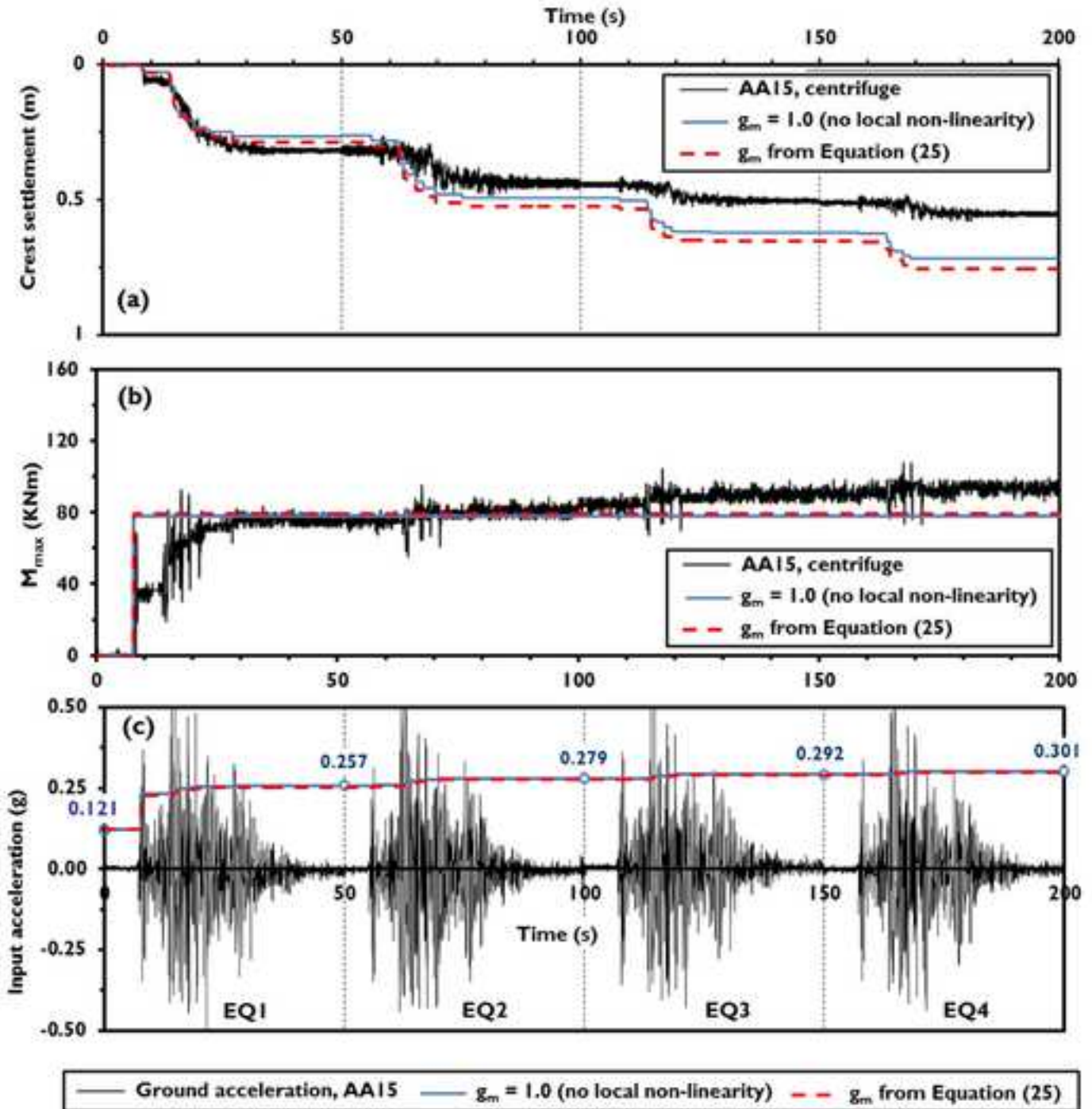


Figure 18

[Click here to download high resolution image](#)

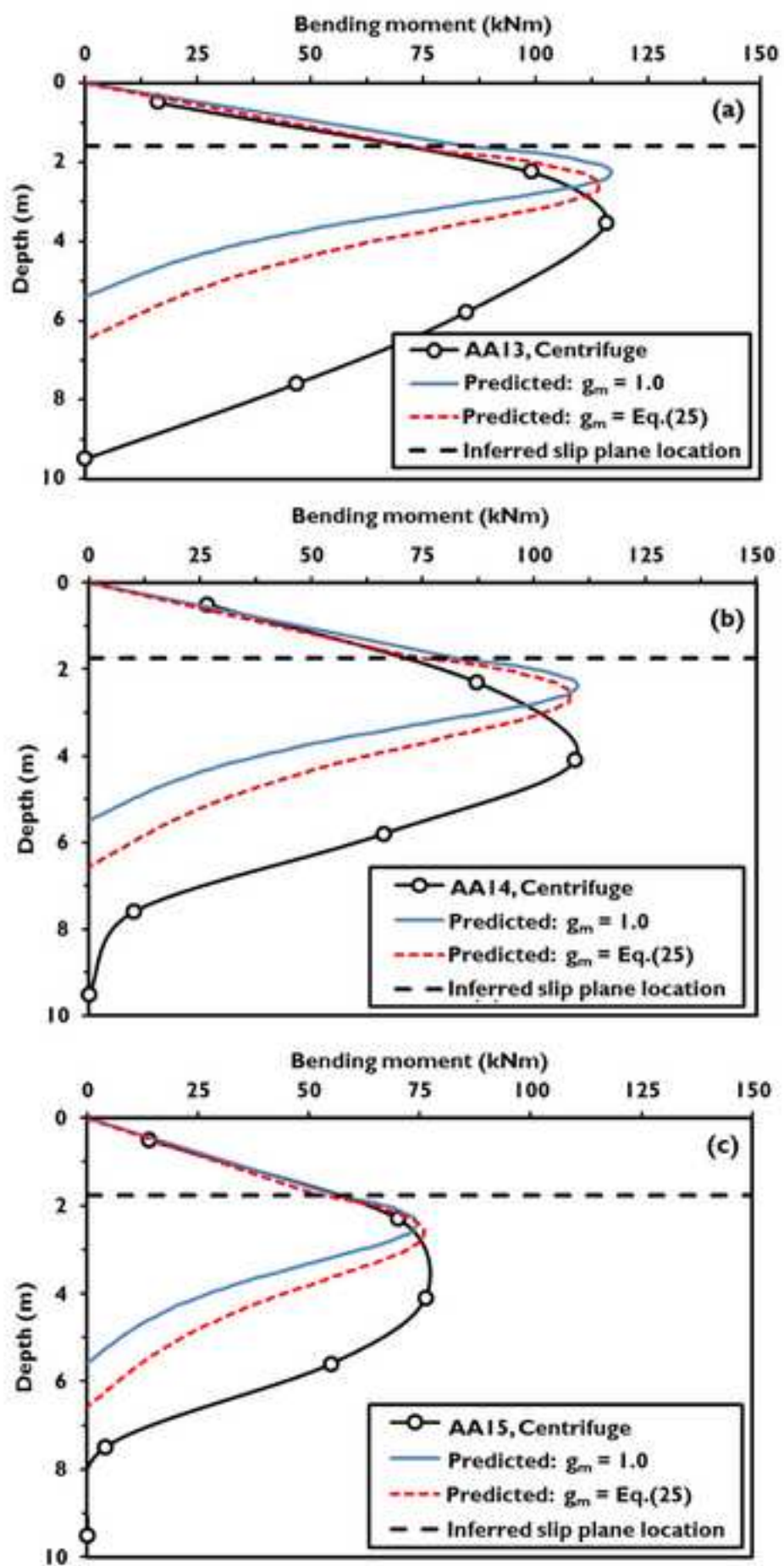


Figure 19
[Click here to download high resolution image](#)

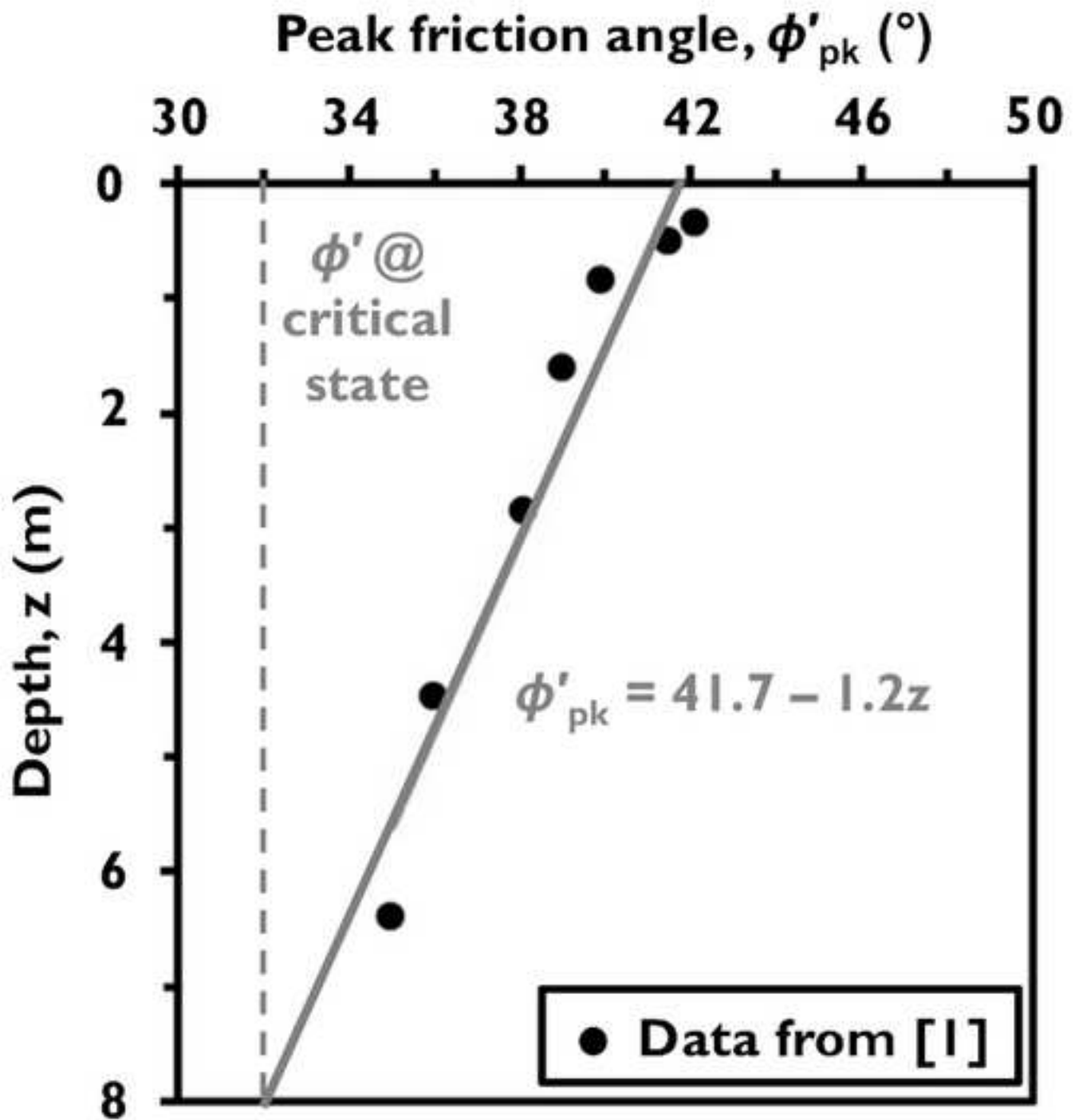


Figure 20

[Click here to download high resolution image](#)

